Ore Geology Reviews 57 (2014) 132–153

Contents lists available at ScienceDirect

Ore Geology Reviews

journal homepage: www.elsevier.com/locate/oregeorev

Petrogenesis of the Mesozoic granites and Mo mineralization of the Luanchuan ore field in the East Qinling Mo mineralization belt, Central China

Zhiwei Bao *, Christina Yan Wang, Taiping Zhao, Chuangju Li, Xinyu Gao

Key Laboratory for Mineralogy and Metallogeny, Guangzhou Institute of Geochemistry, Chinese Academy of Sciences, Guangzhou 510640, China

ARTICLE INFO

Article history:
Received 29 November 2012
Received in revised form 22 August 2013
Accepted 9 September 2013
Available online 18 September 2013

Keywords:
Granite porphyry
Molybdenum mineralization
Mesozoic
Continental crust subduction
East Qinling

ABSTRACT

Numerous Mo deposits associated with the Late Jurassic to Early Cretaceous granite porphyries in the southern margin of the North China Craton make up the East Qinling Mo mineralization belt, one of the most economically important Mo mineralization belt worldwide. Two of the largest porphyry- and skarn-type Mo deposits in the belt are hosted in two granite porphyries in the Luanchuan ore field which emplaced at ~150 Ma and ~135 Ma, respectively. The granite porphyries are calcic–alkalic to alkalic, and metaluminous to peraluminous. They are strongly depleted in Eu, Sr, Ba, P and Ti, indicating that they underwent intensive fractionation of plagioclase, apatite and Fe–Ti oxides. The granite porphyries in the Luanchuan ore field are likely to be connected with nearly coeval Heyu batholith to the east as indicated by the regional geophysical data. The Heyu granite batholith has bulk compositions similar to the granite porphyries, and is possibly a precursor of the granite porphyries. The Heyu granite batholith and granite porphyries have $\varepsilon_{Nd}(t)$ values varying from −11.3 to −17.5 and zircon $\varepsilon_{Hf}(t)$ values from −5.8 to −35.6. They have two-stage Nd modal ages [T_{DM2}(Nd)] ranging from 1.68 to 2.47 Ga and Hf model ages [T_{DM2}(Hf)] from 1.32 to 2.86 Ga, much younger than those for Mesozoic granitoids elsewhere in the eastern part of the North China Craton which are believed to have formed from remelting of the Archean basement. Mesozoic granites in the southern margin of the North China Craton overall have Pb isotope compositions similar to the basement of the Yangtze Block rather than the North China Craton. Therefore, we argue that the granite porphyries and related Mo deposits in the Luanchuan ore field were unlikely sourced from the Taihua Group, instead they may have formed from remelting of the subducted continental crust of the Yangtze Block with T_{DM2}(Nd) ages of ~1.8 to ~2.2 Ga. Partial melts of the subducted continental crust of the Yangtze Block interacted with melts and/or fluids derived from the enriched mantle wedge, which experienced metasomatism due to the dehydration of subducted continental crust of the Yangtze Block, consequently resulting in the formation of the granite porphyries and porphyry- and skarn-type Mo deposits in the Luanchuan ore field.

1. Introduction

Porphyry deposits range from porphyry Cu (±Au, Mo) deposits to porphyry Mo deposits and account for more than 95% of world Mo production and reserves. Two associations of porphyry Mo deposits have been recognized: (1) high-grade, rift-related deposits associated with F-rich and highly evolved rhyolitic stocks; and (2) low-grade, arc-related (or subduction-related) deposits associated with F-poor and calc-alkalic stocks or plutons (e.g., Carten et al., 1993; Sillitoe, 1980).

The East Qinling Mo mineralization belt along the southern margin of the North China Craton in China is one of the most important arc-related Mo mineralization belts, which hosts Mo reserves of ~6 million tons (mt), comparable to the Colorado mineral belt in the USA (Carten et al., 1993). Porphyry- and skarn-type Mo deposits in the belt are often associated with W, Pb, rare earth elements (REE), Au, and U mineralization in the contact zones and/or contiguous areas (Li et al., 2005, 2007; Mao et al., 2002; Shi et al., 2009; Yang et al., 2009a, 2009b).

The origin of porphyry- and skarn-type Mo deposits in the East Qinling Mo mineralization belt and associated Mesozoic granites in the southern margin of the North China Craton have been extensively investigated and debated in the past two decades (e.g., Bao et al., 2009a; Chen et al., 2000; Gao et al., 2010; Li et al., 2007, 2009a, 2009b; Luo et al., 1991; Mao et al., 2008, 2010). Some researchers believed that the Mesozoic granites were derived from remelting of the crystalline basement of the North China Craton that is composed of the Archean Taihua Group in this region (e.g., Chen et al., 2000), whereas other workers suggested that the source rocks could be the lower crust with the involvement of the upper mantle (e.g., Luo et al., 1993; Sun and Liu, 1987; Zhang et al., 2010; Zhu et al., 2010a). A few workers argued that the ore-bearing and barren granites are genetically different, belonging to I-type and S-type, respectively (e.g., Lu et al., 2002), whereas other studies proposed that the Jurassic to Early Cretaceous granites (~150–

* Corresponding author.
E-mail address: baozw@gig.ac.cn (Z. Bao).

0169-1368/$ – see front matter © 2013 Elsevier B.V. All rights reserved.
http://dx.doi.org/10.1016/j.oregeorev.2013.09.008

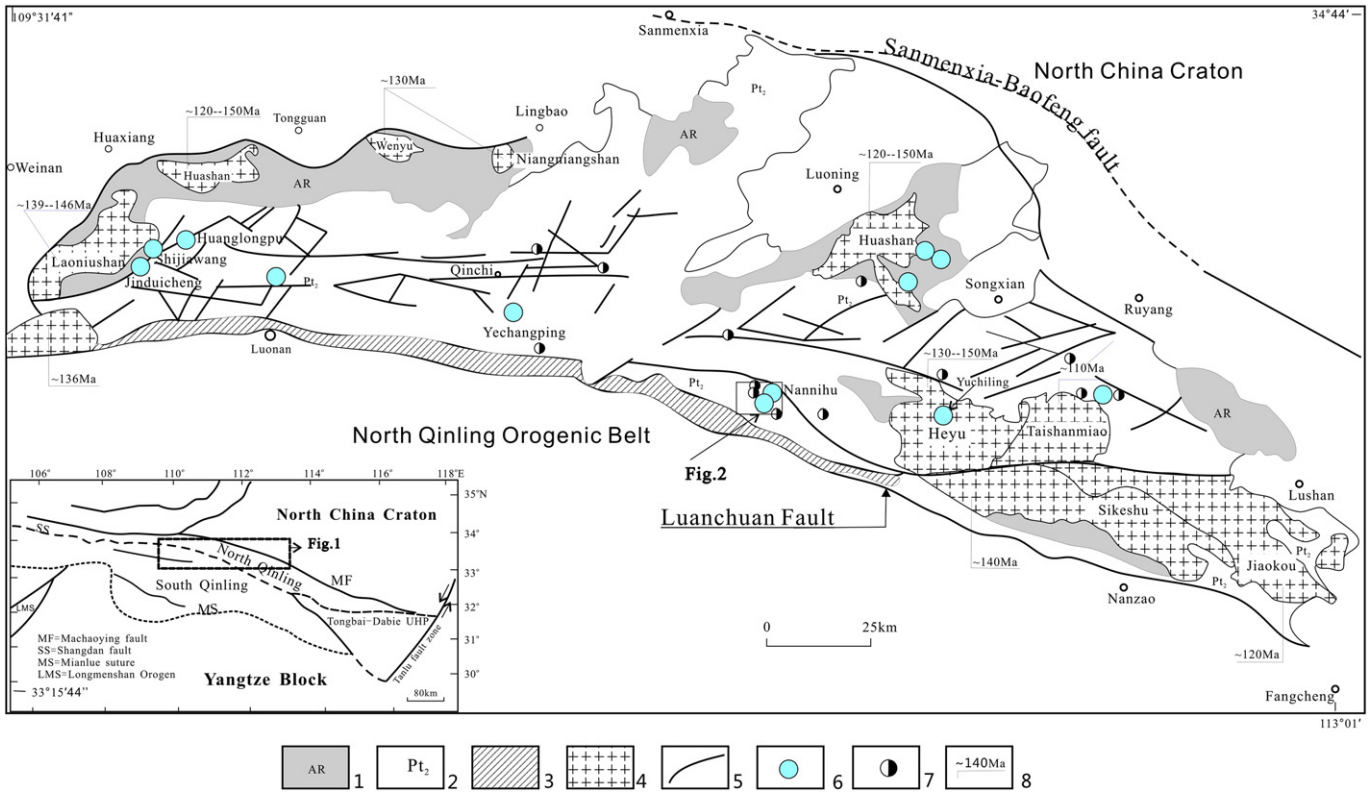

Fig. 1. Simplified geological map showing the distribution of Mesozoic granites and related Mo deposits in East Qinling orogenic belt, Central China (modified after Meng and Zhang, 2000 and Mao et al., 2008). — 1. Archean metamorphic rocks; 2. Mesoproterozoic strata; 3. Neoproterozoic strata; 4. Mesozoic granite; 5. Fault; 6. Porphyry-skarn-type Mo deposit; 7. Pb–Zn–Ag deposit; and 8. Ages of granite plutons and mineralization.

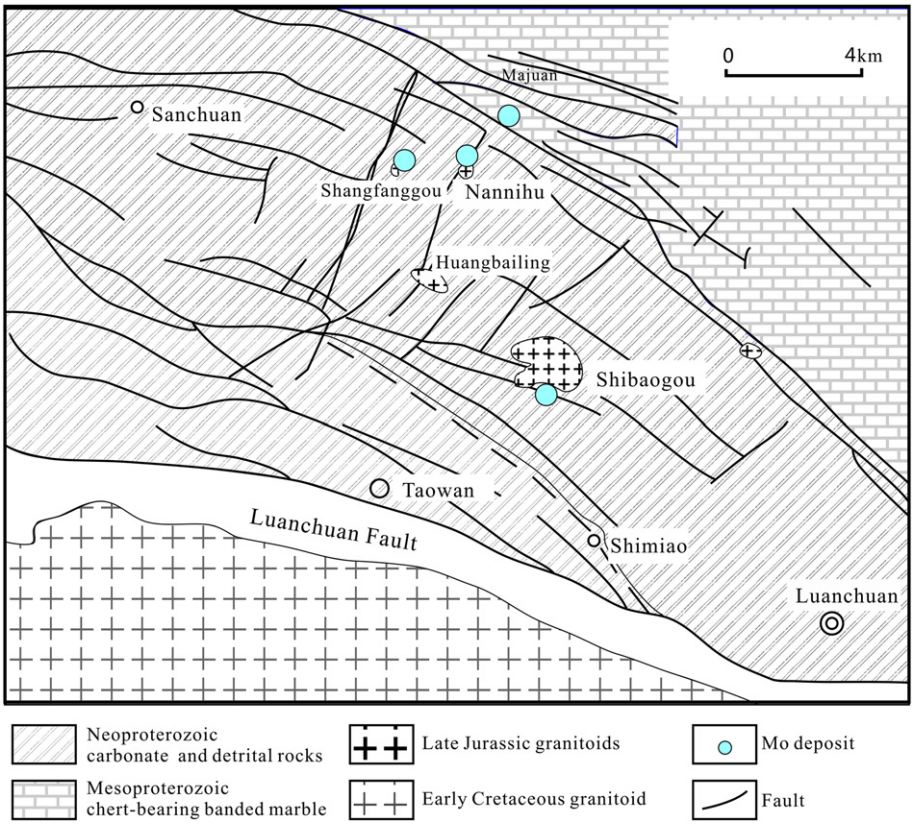

Fig. 2. Simplified map showing the distribution of granite porphyry-type and skarn-type molybdenum deposits in the Luanchuan ore field. Modified after Mao et al. (2009).

~135 Ma) were derived mainly from partial melting of subducted continental crust of the Yangtze Block (Bao et al., 2009a; Li et al., 2012a).

Emplacement of granite plutons and associated Mo mineralization in the East Qinling Mo mineralization belt were considered to be related to the switch of geodynamic regimes in the Late Mesozoic in East China due to a shift from oblique, shallow subduction of the Izanagi Plate to orthogonal, steep subduction of the Paleo-Pacific Plate, leading to the lithospheric thinning of the North China Craton (Hou et al., 2010; Sun et al., 2007; Wu et al., 2008; Zhu et al., 2010b). In this fashion, the Jurassic to Early Cretaceous (>131 Ma) granites are considered to be related to the transformation of the tectonic regime from NS- to nearly EW-directions in East China, i.e., a continental margin arc setting controlled by the subduction of the Izanagi or Paleo-Pacific plate beneath the Eurasian continent in a WNW–ESE direction in the Late Jurassic–Early Cretaceous, whereas the emplacement of younger granites (<131 Ma) can be ascribed to large-scale lithospheric thinning beneath the North China Craton (Guo et al., 2013; Li et al., 2005, 2013a,b; Mao et al., 2005, 2008, 2010; Zhang et al., 2010). Other workers suggested that the Late Jurassic to Early Cretaceous granites in the East Qinling resulted from remelting of the lower crust in post-orogenic stage (Zhu et al., 2010a) or remelting of subducted crust in post-collisional setting (Bao et al., 2009a; Li et al., 2012a).

The source of Mo is also a matter of debate. Many researchers believe that Mo was mainly derived from the lower crust, or from the Archean basement and Paleoproterozoic rocks of the North China Craton (e.g., Liu et al., 2007; Lu et al., 2002). Some others propose that the carbonaceous sedimentary rocks may be the main source for the Mo mineralization (e.g., Li et al., 2012b; Zhang et al., 2010). A few researchers recognized that the upper mantle could be the major source for Mo mineralization because of high Mo concentrations of the upper mantle in the southern margin of the North China Craton (Bao et al., 2009a; Zhu et al., 2010a).

In the Luanchuan ore field, the most economically important Mo producer in the East Qinling Mo mineralization belt, where the ore-bearing granite porphyries are nearly coeval with the adjacent Heyu granite batholith, and have bulk compositions similar to the Heyu granite batholith. However, a genetic link between them has not yet been examined. In this paper, we report zircon U/Pb ages and Lu–Hf isotope composition, whole-rock major and trace elements, and Sm–Nd isotopic compositions of ore-bearing granite porphyries and the Heyu granite batholith. The data set enables us to examine the relationship of the ore-bearing granite porphyries and Heyu granite batholith and to delineate the source rocks of the ore-bearing granite porphyries in this region and the source of Mo.

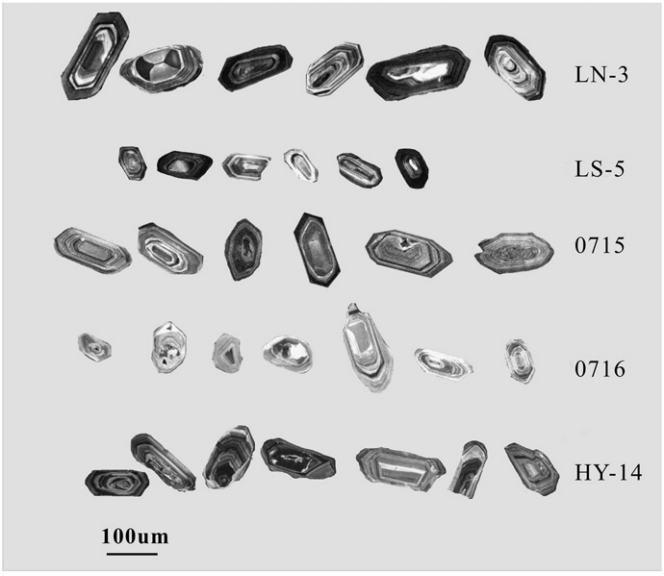

Fig. 3. Cathodoluminescence images of representative zircon grains from the ore-bearing granite porphyries in the Luanchuan ore field and the Heyu batholith.

2. Geological background

The Central China orogenic belt is bound by the North China Craton to the north and the Yangtze Block to the south and extends more than 4000 km from West Kunlun on the west, through Qilian, West Qinling, East Qinling and Dabie, to Sulu on the east (Yang et al., 2002). The belt had experienced a prolonged divergence and convergence between blocks and preserved a record of the Late Mesoproterozoic to Cenozoic tectonism (Meng and Zhang, 1999, 2000; Ratschbacher et al., 2003) (Fig. 1).

The East Qinling segment of the Central China orogenic belt is composed of four blocks, from north to south, including the southern margin of the North China Craton, North Qinling Block, South Qinling Block, and the northern margin of the Yangtze Block. The four blocks are separated by the Luanchuan fault, Shangdan and Mianlue sutures, respectively. The North Qinling Block can be further divided into the Kuanping unit, Erlangping unit, and North Qinling unit, whereas the South Qinling Block can be subdivided into the Shangdan ophiolite unit, Liuling flysch unit, Douling low-grade metamorphic rock unit, and South Qinling unit. There are three episodes of arc–continent collision during the Paleozoic continental convergence between the Yangtze Block and North China Craton. The first-episode of collision was caused by northward subduction of the North Qinling, resulting in UHP metamorphism at ca. 480–490 Ma and the accretion of the North Qinling to the North China Craton. The second episode of collision involved the northward subduction of the Proto-Tehyan oceanic crust beneath an Andes-type continental arc, leading to granulite-facies metamorphism at ca. 420–430 Ma and the accretion of the Shangdan arc terrane to the North China Craton. The third-episode collision is caused by northward subduction of the Paleo-Tethyan oceanic crust, resulting in the low-P metamorphism in the Qinling orogen as well as crustal accretion to the NCB. The massive continental subduction of the Yangtze Block beneath the North China Craton took place in the Triassic collision with the final continent–continent collision along the Mianlue suture (Meng and Zhang, 1999; Wu and Zheng, 2013 and references therein).

The southern margin of the North China Craton is separated from the Kuanping unit by the Luanchuan fault in the south. The southern margin of the North China Craton in East Qinling consists mainly of an Archaean (~2.5 to ~2.8 Ga) basement and it is unconformably overlain by the Proterozoic volcanic and sedimentary sequences. The Archean basement is composed of the amphibolite- to granulite-facies metamorphic rocks of the Taihua Group. The Proterozoic volcanic and sedimentary sequences consist of the Paleoproterozoic mafic to felsic volcanic rocks and minor sedimentary rocks of the Xiong'er Group, Mesoproterozoic quartzite and schist with intercalated dolomitic marble of the Guandaokou Group, and Neoproterozoic Luanchuan Group that is composed, from the basement upwards, of meta-sandstone of the Sanchuan Formation, the marble and schist of the Nannihu Formation, and the dolomitic marble of the Meiyaogou Formation.

The North Qinling unit consists mainly of deformed Paleoproterozoic biotite plagioclase gneiss, granulite, amphibolite, thin layers of graphite marbles, and Paleozoic to Mesozoic granitic plutons in the lower part and a thick pile of gently folded Paleozoic marble in the upper part (Dong et al., 2011; Xue et al., 1996). The tectonic affinity of the North Qinling has been debated, and at least three different models are proposed; 1) it was the southern margin of the North China Craton (Meng and Zhang, 1999); 2) its lower unit was correlated with the basement of the Yangtze Block and its upper unit with the North China Craton (Ratschbacher et al., 2003; Xue et al., 1996); or 3) it was an independent microcontinent intervening between the Yangtze Block and North China Craton (Ouyang and Zhang, 1996). Recent study on detrital zircons indicates that the North Qinling was separated from the

Table 1
LA-ICPMS zircon U–Pb ages of the Nannihu granite porphyry.

Spots	Pb* (ppm)	Th (ppm)	U (ppm)	Th/U	$^{207}Pb/^{206}Pb \pm 1\sigma$	$^{207}Pb/^{235}U \pm 1\sigma$	$^{206}Pb/^{238}U \pm 1\sigma$	$^{207}Pb/^{235}U$ age $\pm 1\sigma$ (Ma)	$^{206}Pb/^{238}U$ age $\pm 1\sigma$ (Ma)
LN-3.01	252	578	2284	0.25	0.05210 ± 64	0.1698 ± 15	0.02364 ± 13	159 ± 1	150.6 ± 0.8
LN-3.02	402	2553	3499	0.73	0.04944 ± 55	0.1583 ± 12	0.02322 ± 12	149 ± 1	148.0 ± 0.8
LN-3.03	361	1535	3236	0.47	0.05017 ± 57	0.1614 ± 12	0.02333 ± 12	152 ± 1	148.7 ± 0.8
LN-3.04	281	1279	2478	0.52	0.04953 ± 57	0.1607 ± 12	0.02353 ± 12	151 ± 1	149.9 ± 0.8
LN-3.05	242	1013	2170	0.47	0.04951 ± 62	0.1588 ± 14	0.02326 ± 13	150 ± 1	148.2 ± 0.8
LN-3.06	361	1842	3178	0.58	0.04986 ± 57	0.1611 ± 12	0.02343 ± 12	152 ± 1	149.3 ± 0.8
LN-3.07	362	1050	3307	0.32	0.04959 ± 58	0.1597 ± 13	0.02336 ± 12	150 ± 1	148.9 ± 0.8
LN-3.08	325	1310	2897	0.45	0.04904 ± 58	0.1588 ± 13	0.02348 ± 12	150 ± 1	149.6 ± 0.8
LN-3.09	94.3	657.6	801.9	0.82	0.06068 ± 88	0.1964 ± 22	0.02347 ± 13	182 ± 2	149.5 ± 0.8
LN-3.10	298	838.4	2389	0.35	0.04968 ± 84	0.1814 ± 26	0.02648 ± 16	169 ± 2	168.0 ± 1
LN-3.11	379	1531	3347	0.46	0.04932 ± 57	0.1617 ± 13	0.02377 ± 12	152 ± 1	151.4 ± 0.8
LN-3.12	227	1562	1947	0.8	0.04874 ± 68	0.1576 ± 17	0.02345 ± 13	149 ± 2	149.4 ± 0.8
LN-3.13	110	661.3	940	0.7	0.05205 ± 80	0.1695 ± 21	0.02361 ± 14	150 ± 3	149.9 ± 0.9
LN-3.14	252	77.3	1582	0.05	0.04871 ± 66	0.1592 ± 16	0.02371 ± 13	150 ± 1	151.1 ± 0.8
LN-3.15	226	865	2016	0.43	0.04923 ± 73	0.1605 ± 19	0.02365 ± 13	151 ± 2	150.7 ± 0.8
LN-3.16	252	1751	2634	0.66	0.04837 ± 55	0.1569 ± 12	0.02352 ± 12	148 ± 1	149.9 ± 0.8
LN-3.17	265	1194	2368	0.5	0.04926 ± 59	0.1593 ± 13	0.02345 ± 12	150 ± 1	149.4 ± 0.8
LN-3.18	252	947.4	1638	0.58	0.05100 ± 80	0.1547 ± 20	0.02200 ± 13	146 ± 2	140.3 ± 0.8
LN-3.19	194	1608	1662	0.97	0.04945 ± 68	0.1591 ± 17	0.02332 ± 13	150 ± 1	148.6 ± 0.8
LN-3.20	252	1178	1104	1.07	0.05384 ± 96	0.1571 ± 24	0.02116 ± 13	148 ± 2	135.0 ± 0.8
LN-3.21	306	1040	2820	0.37	0.04938 ± 62	0.1582 ± 14	0.02323 ± 12	149 ± 1	148.0 ± 0.8
LN-3.22	252	1525	1871	0.82	0.04895 ± 59	0.1586 ± 14	0.02349 ± 12	149 ± 1	149.7 ± 0.8
LN-3.23	188	1080	1782	0.61	0.05139 ± 72	0.1552 ± 17	0.02189 ± 12	146 ± 1	139.6 ± 0.8
LN-3.24	183	688	1657	0.42	0.04928 ± 68	0.1604 ± 17	0.02361 ± 13	151 ± 2	150.4 ± 0.8
LN-3.25	200	967.3	1906	0.51	0.04829 ± 70	0.1469 ± 17	0.02206 ± 12	139 ± 2	140.7 ± 0.8
LN-3.26	1174	489.6	873.5	0.56	0.09862 ± 99	3.65 ± 19	0.2686 ± 14	1547 ± 7	1531 ± 7
LN-3.27	262	1047	2556	0.41	0.05012 ± 69	0.1508 ± 16	0.02182 ± 12	143 ± 1	139.1 ± 0.8
LN-3.28	117	1091	1082	1.01	0.0512 ± 10	0.1497 ± 27	0.02118 ± 14	136 ± 4	134.7 ± 0.9
LN-3.29	399	1433	3950	0.36	0.05084 ± 66	0.1518 ± 15	0.02165 ± 12	144 ± 1	138.1 ± 0.8
LN-3.30	186	773.4	1790	0.43	0.04893 ± 65	0.1490 ± 15	0.02208 ± 12	141 ± 1	140.8 ± 0.8
LN-3.31	192	1435	1797	0.8	0.05108 ± 72	0.1522 ± 17	0.02161 ± 12	144 ± 1	137.8 ± 0.8
LN-3.32	266	1135	2665	0.43	0.05171 ± 81	0.1524 ± 19	0.02137 ± 12	144 ± 2	136.3 ± 0.8
LN-3.33	227	1299	2187	0.59	0.04975 ± 69	0.1474 ± 16	0.02147 ± 12	140 ± 1	136.9 ± 0.8
LN-3.34	263	947.4	2533	0.37	0.05181 ± 76	0.1587 ± 19	0.02221 ± 12	145 ± 2	141.3 ± 0.8
LN-3.35	269	608.5	2698	0.23	0.05717 ± 69	0.1692 ± 14	0.02145 ± 11	159 ± 1	136.8 ± 0.7

Yangtze Block during the Rodinian breakup and then became a micro-continent intervening between the Yangtze Block and North China Craton (Wu and Zheng, 2013).

The Luanchuan ore field in the southern margin of the North China Craton hosts ~3 mt of proven Mo reserve (Fig. 2). Ore-bearing granite porphyries intruded the Mesoproterozoic Guandaokou Group and Neoproterozoic Luanchuan Group. Some nearly coeval, enriched mantle-derived mafic dikes also occur in the ore field (Bao et al., 2009b). The Heyu granite batholith is located 40 km east of the Luanchuan ore field, and is bounded by the Machaoying fault to the north and the Luanchuan fault to the south.

2.1. Ore-bearing granite porphyries in the Luanchuan ore field

Mesozoic granite porphyries that host Mo mineralization in the Luanchuan ore field are usually small bodies with outcrop areas <1 km^2. The granite porphyries are mainly composed of K-feldspar, biotite, quartz and plagioclase. K-feldspar is a common phenocryst and is of either magmatic or altered origin. Magmatic K-feldspar is either subhedral to anhedral orthoclase or microcline, which often contains fine albite stripes and Carlsbad twins. Altered K-feldspars commonly occur along the fractures, rims and cleavages of plagioclase, and also occur as vein or veinlet. Magnesian biotite mainly occurs in the groundmass, and was partly altered to chlorite, sericite, magnetite, and rutile. Quartz occurs in both groundmass and phenocryst, and rounded quartz phenocryst shows undulance extinction. Plagioclase laths are commonly oligoclase with minor andesine and albite. Accessory minerals include magnetite, apatite, sphene, zircon, thorite, rutile, and pyrite.

The Nannihu, Shangfanggou, and Shibaogou granite porphyries host economic Mo deposits in the Luanchuan ore field. Disseminated ores occur as thin flakes along fractures or fine pieces in veinlets of porphyry ores and skarn-type ores. Ore minerals are composed of molybdenite, sheelite, pyrite, pyrrhotite, and chalcopyrite, with minor sphalerite, bornite, magnetite, and hematite. Gangue minerals include garnet, diopside, quartz, wollastonite, phlogopite, talc, serpentine, chlorite, fluorite, and calcite. A few coeval vein- and skarn-type Pb, Zn and Ag deposits occur adjacent to these Mo deposits (Bao et al., 2009b; Yan, 2004).

The Nannihu granite porphyry occurs as a small stock with an exposure area of ~0.12 km^2. Available drill core profiles indicate that the stock is dilated to 1.2 km^2 at a depth of 900 m (Liu et al., 2006). The Nannihu granite porphyry intruded the meta-sandstone, siltstone, and argillaceous limestone of the Luanchuan Group which were altered to hornfels, marble and skarn. The porphyry body consists mainly of fine- to medium-grained porphyritic monzogranite near the surface and fine-grained porphyritic biotite granodiorite at depth, and contains a proven Mo reserve of ~2 mt. Porphyritic monzogranite contains 20–50% phenocryst with grains ranging in size from 5 to 12 mm. The phenocryst consists mainly of orthoclase, bipyramid quartz and plagioclase (An = ~20). Groundmass shows microgranitic texture and is composed of 30–35% orthoclase perthite, 25–35% quartz, and 1–3% biotite. Porphyritic biotite granodiorite contains 5–10% phenocryst composed of orthoclase perthite (5–10 mm), euhedral and zoned plagioclase, and quartz. The groundmass shows fine- to micro-granitic (0.1–1 mm) texture and consists of K-feldspar, quartz and biotite. Accessory minerals include magnetite, sphene, apatite, rutile, monazite, garnet, and zircon. The Nannihu granite porphyry was dated at 142 ± 15 Ma using Rb–Sr isochron method (Hu et al., 1988), however, the age is questionable because the Rb–Sr system of the rocks may have been disturbed by intensive late-stage hydrothermal alteration. Mo mineralization is mainly hosted in porphyry, biotite-bearing calcite–silicate hornfels, actinolite- and diopside-bearing

calcite–silicate hornfels, diopside hornfels, and skarn. Four molybdenite samples yield Re–Os model ages ranging from 142 ± 2 Ma to 145 ± 2 Ma (Li et al., 2006).

The ~0.05 km^2 Shangfanggou granite porphyry intruded the dolomitic marble with intercalated carbonaceous schist of the Luanchuan Group. It consists of porphyritic syenogranite and minor porphyritic biotite granite and contains a proven Mo reserve of ~0.72 mt. The porphyritic syenogranite contains 15–25% phenocryst. The phenocrysts are commonly smaller than 3 mm in size and consist of K-feldspar, plagioclase, quartz and biotite, whereas groundmass shows micro- to fine-grained granitic texture or micrographic texture. Accessory minerals include apatite, zircon, magnetite, scheelite, pyrite, rutile, ilmenite and sphene. The porphyritic syenogranite is intensively silicified, especially at the margin of the porphyritic pluton. The ore bodies occur within the porphyry and surrounding magnesian skarn. Skarn-type Fe mineralization occurs in the contact zone of the porphyric body and dolomitic marble and is associated with low-grade Mo ores. The porphyry was dated to be 134 ± 2 Ma using whole-rock Rb–Sr isochron method (Hu et al., 1988). Two molybdenite samples from the porphyry- and skarn-type ores yield Re–Os model ages of 144 ± 2 Ma and 146 ± 2 Ma, respectively (Li et al., 2006).

The Shibaogou granite porphyry is the largest one in the ore field and crops out in an area of ~3 km^2. It consists mainly of the early-stage coarse- to medium-grained monzogranite and late-stage fine-grained syenogranite. It intruded the meta-sandstone, marble, schist and quartzite of the Luanchuan Group. The monzogranite consists mainly of 20–40% K-feldspar, 15–30% plagioclase, 15–35% quartz and 2–5% biotite. The mineral grains range in size from ~5 mm in the northeastern margin to ~0.2 mm in the northwestern margin of the pluton. K-feldspars are commonly subhedral to anhedral and show Carlsbad twins and occasionally cross hatched twin. Euhedral to subhedral plagioclase shows polysynthetic twin and is sometimes weakly sericitized. Anhedral quartz commonly shows undulatory extinction. Biotite is often chloritized. Accessory minerals include sphene, apatite, zircon and magnetite. The Shibaogou granite porphyry hosts a small-sized Mo deposit with a Mo reserve of ~0.14 mt. The ore bodies occur along the contact zone of the porphyry body and the marble of the Luanchuan Group. Disseminated ores, and ore-bearing quartz veins or stockwork occur within the porphyry, skarn and hornfels of the wall rocks. A whole-rock Rb–Sr isochron age of 143 ± 7 Ma was obtained for the Shibagou granite (Yang et al., 1997). Recently the porphyritic monzogranite and fine-grained monzogranite are dated to be 156 ± 1 Ma and 157 ± 1 Ma by LA-ICPMS zircon U/Pb dating technique, respectively (Yang et al., 2012a). Six molybdenite samples from the porphyry- and skarn-type ores yielded Re–Os model ages ranging from 142 ± 2 Ma to 147 ± 3 Ma (Mao et al., 2008).

A few E–W or NWW striking mafic dikes occur in the ore field and range from a few centimeters to a few meters in thickness. The mafic

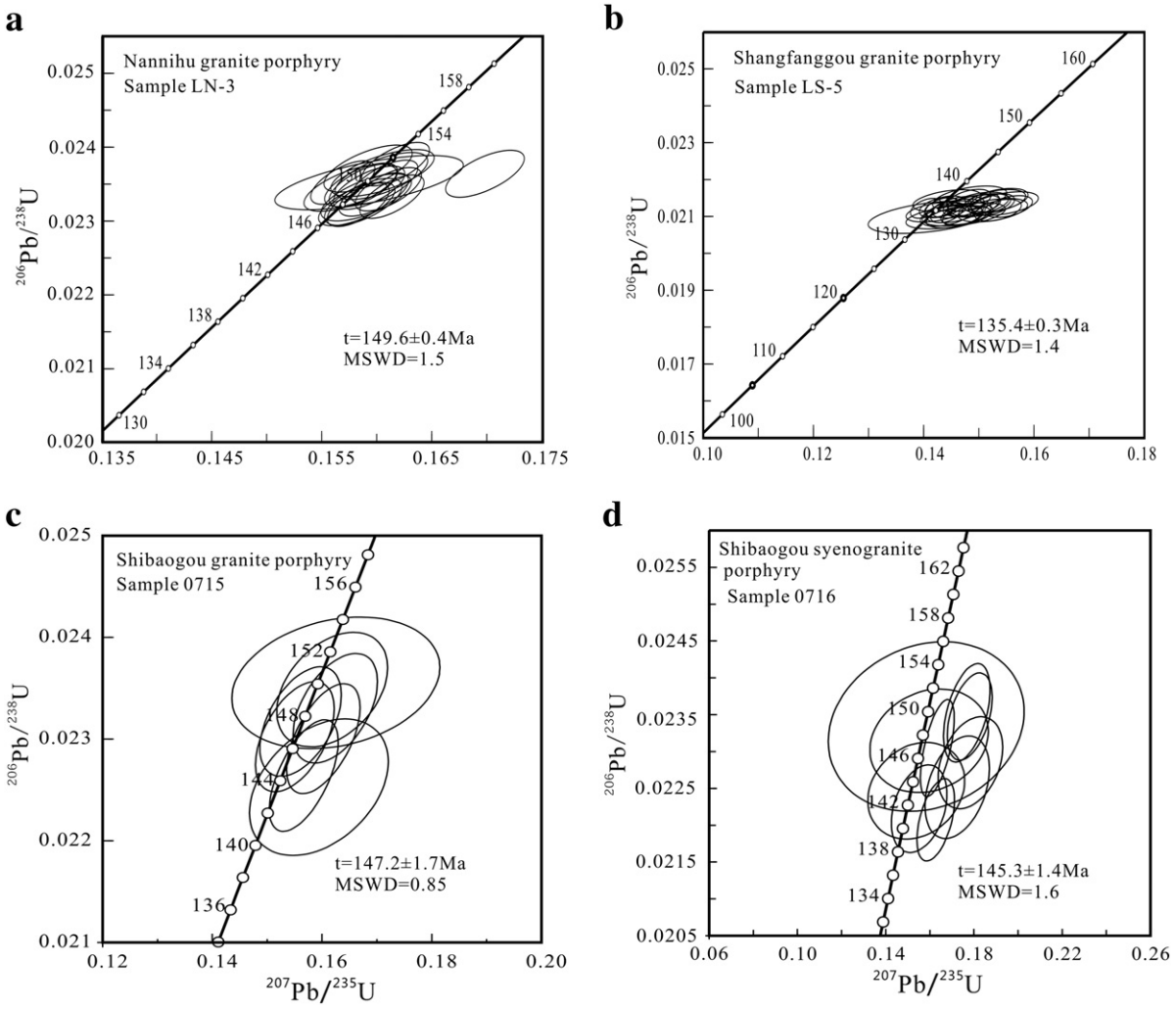

Fig. 4. Concordia plots of the zircons from the granite porphyries in the Luanchuan ore field.

Table 2
LA-ICPMS zircon U–Pb ages of the Shangfanggou granite porphyry.

Test no.	Pb* (ppm)	Th (ppm)	U (ppm)	Th/U	$^{207}Pb/^{206}Pb \pm 1\sigma$	$^{207}Pb/^{235}U \pm 1\sigma$	$^{206}Pb/^{238}U \pm 1\sigma$	$^{207}Pb/^{235}U$ age $\pm 1\sigma$ (Ma)	$^{206}Pb/^{238}U$ age $\pm 1\sigma$ (Ma)
LS-5.01	137	768.1	1244	0.62	0.04996 ± 88	0.1457 ± 22	0.02115 ± 13	138 ± 2	134.9 ± 0.8
LS-5.02	344	1571	3511	0.45	0.05224 ± 85	0.1383 ± 19	0.01920 ± 11	128 ± 2	122.4 ± 0.7
LS-5.03	138	968.3	1227	0.79	0.04991 ± 80	0.1462 ± 19	0.02125 ± 12	139 ± 2	135.6 ± 0.8
LS-5.04	573	1965	5442	0.36	0.04969 ± 80	0.1442 ± 19	0.02103 ± 12	137 ± 2	134.2 ± 0.8
LS-5.05	349	1396	3227	0.43	0.05093 ± 89	0.1499 ± 23	0.02134 ± 13	142 ± 2	136.1 ± 0.8
LS-5.06	354	1724	3284	0.52	0.05256 ± 76	0.1535 ± 17	0.02117 ± 12	145 ± 2	135 ± 0.8
LS-5.07	484	1675	4644	0.36	0.05035 ± 86	0.1457 ± 21	0.02098 ± 12	138 ± 2	133.8 ± 0.8
LS-5.08	206	1515	1809	0.84	0.05066 ± 86	0.1487 ± 21	0.02129 ± 12	141 ± 2	135.8 ± 0.8
LS-5.09	512	1547	4849	0.32	0.05177 ± 91	0.1529 ± 23	0.02141 ± 13	144 ± 2	136.6 ± 0.8
LS-5.10	47	858	2176	0.39	0.04885 ± 16	0.03065 ± 95	0.00455 ± 4	30.7 ± 0.9	29.3 ± 0.3
LS-5.11	255	1858	2271	0.82	0.05012 ± 71	0.1482 ± 17	0.02144 ± 12	140 ± 1	136.8 ± 0.8
LS-5.12	178	1077	1772	0.61	0.05241 ± 85	0.14131 ± 19	0.01955 ± 11	134 ± 2	124.8 ± 0.7
LS-5.13	487	2123	4643	0.46	0.04797 ± 57	0.1404 ± 12	0.02122 ± 11	133 ± 1	135.4 ± 0.7
LS-5.14	210	1213	1944	0.62	0.04890 ± 73	0.1434 ± 17	0.02126 ± 12	136 ± 2	135.6 ± 0.8
LS-5.15	150	345.6	1168	0.3	0.0554 ± 15	0.2005 ± 52	0.02625 ± 21	174 ± 5	166 ± 1
LS-5.16	200	2084.6	1778	1.17	0.05296 ± 77	0.1554 ± 18	0.02127 ± 12	147 ± 2	135.7 ± 0.8
LS-5.17	532	2155	5157	0.42	0.04955 ± 60	0.1442 ± 12	0.02110 ± 11	137 ± 1	134.6 ± 0.7
LS-5.18	232	1396	2246	0.62	0.05347 ± 89	0.1502 ± 21	0.02036 ± 12	142 ± 2	129.9 ± 0.8
LS-5.19	173	1723	1518	1.14	0.05083 ± 79	0.1477 ± 19	0.02107 ± 12	140 ± 2	134.4 ± 0.8
LS-5.20	452	1574	4412	0.36	0.05071 ± 67	0.1471 ± 15	0.02102 ± 11	139 ± 1	134.1 ± 0.7
LS-5.21	606	1971	2306	0.85	0.0964 ± 13	0.6392 ± 63	0.04809 ± 28	502 ± 4	303 ± 2
LS-5.22	185	1317	1730	0.76	0.05229 ± 78	0.1522 ± 18	0.02110 ± 12	140 ± 3	134.3 ± 0.8
LS-5.23	86	685.3	774.2	0.89	0.05253 ± 98	0.1547 ± 25	0.02135 ± 13	146 ± 2	136.2 ± 0.8
LS-5.24	106	1195	922.7	1.3	0.0523 ± 10	0.1525 ± 26	0.02117 ± 13	144 ± 2	135 ± 0.8
LS-5.25	120	561.1	1248	0.45	0.05226 ± 91	0.1429 ± 21	0.01983 ± 12	128 ± 3	126.1 ± 0.8
LS-5.26	182	1485	1642	0.9	0.0501 ± 10	0.1483 ± 27	0.02148 ± 14	140 ± 2	137 ± 0.9
LS-5.27	463	1931	4532	0.43	0.04886 ± 59	0.1432 ± 12	0.02125 ± 11	136 ± 1	135.6 ± 0.7
LS-5.28	503	1540	5025	0.31	0.04892 ± 61	0.1433 ± 13	0.02124 ± 11	136 ± 1	135.5 ± 0.7
LS-5.29	207	1435	1983	0.72	0.05131 ± 78	0.1488 ± 18	0.02102 ± 12	137 ± 3	133.9 ± 0.8
LS-5.30	230	1122	2239	0.5	0.05183 ± 73	0.1524 ± 17	0.02132 ± 12	144 ± 1	136 ± 0.8
LS-5.31	121	794.5	1172	0.68	0.0488 ± 17	0.1413 ± 46	0.02098 ± 18	134 ± 4	134 ± 1
LS-5.32	461	1328	4586	0.29	0.05188 ± 90	0.1534 ± 23	0.02144 ± 13	145 ± 2	136.8 ± 0.8
LS-5.33	484	2145	4735	0.45	0.05011 ± 76	0.1484 ± 18	0.02147 ± 12	137 ± 2	136.7 ± 0.8
LS-5.34	396	2125	3895	0.55	0.05037 ± 64	0.1469 ± 13	0.02116 ± 11	135 ± 2	134.7 ± 0.7
LS-5.35	117	934.8	1148	0.81	0.04974 ± 97	0.1416 ± 24	0.02064 ± 13	134 ± 2	131.7 ± 0.8
LS-5.36	316	1280	3001	0.43	0.04900 ± 87	0.1511 ± 23	0.02236 ± 13	143 ± 2	142.6 ± 0.8
LS-5.37	466	1600	4694	0.34	0.05108 ± 93	0.1500 ± 23	0.02130 ± 13	142 ± 2	135.9 ± 0.8
LS-5.38	430	2119	4244	0.5	0.05127 ± 6	0.1509 ± 12	0.02134 ± 11	143 ± 1	136.1 ± 0.7
LS-5.39	600	2023	6226	0.32	0.04987 ± 66	0.1435 ± 14	0.02087 ± 11	133 ± 2	133 ± 0.7

Table 3
SHRIMP zircon U–Pb ages of the Shibaogou granite porphyry.

Spot	U (ppm)	Th (ppm)	$^{232}Th/^{238}U$	$^{206}Pb^*$ (ppm)	$^{206}Pb/^{238}U$ age (Ma)	$^{207}Pb^*/^{206}Pb^*$	±%	$^{207}Pb^*/^{235}U$	±%	$^{206}Pb^*/^{238}U$	±%	Err corr
Biotite granite porphyry												
0715-1	801	428	0.55	15.6	144.3 ± 2.3	0.0502	2.1	0.1567	2.6	0.02264	1.6	0.607
0715-2	855	931	1.12	17.0	146.6 ± 2.2	0.0505	2.3	0.1602	2.8	0.02300	1.6	0.563
0715-3	878	319	0.38	17.4	146.7 ± 2.3	0.0488	2.6	0.1550	3.1	0.02302	1.6	0.508
0715-4	531	459	0.89	9.81	136.8 ± 2.2	0.0491	3.2	0.1453	3.6	0.02145	1.6	0.457
0715-5	1147	335	0.30	22.9	147.7 ± 2.2	0.0489	2.7	0.1561	3.1	0.02317	1.5	0.490
0715-6	776	639	0.85	15.1	143.6 ± 2.8	0.0513	4.9	0.1594	5.2	0.02253	2.0	0.375
0715-7	850	444	0.54	17.3	149.7 ± 2.3	0.0500	3.8	0.1619	4.1	0.02349	1.6	0.384
0715-8	1168	526	0.46	21.0	132.9 ± 2.3	0.0484	2.8	0.1391	3.3	0.02083	1.8	0.525
0715-9	1277	692	0.56	25.7	148.5 ± 2.2	0.0505	2.7	0.1624	3.1	0.02330	1.5	0.488
0715-10	579	280	0.50	11.9	150.1 ± 2.7	0.0500	7.5	0.163	7.7	0.02355	1.8	0.235
Shibaogou fine-grained syenogranite												
0716-1	145	198	1.41	3.02	148.7 ± 4.8	0.0492	18	0.158	19	0.02334	3.3	0.176
0716-2	268	608	2.35	5.22	143.2 ± 2.7	0.0497	9.2	0.154	9.4	0.02247	1.9	0.205
0716-3	343	288	0.87	51.7	1041 ± 15	0.08649	0.93	2.091	1.8	0.1753	1.6	0.861
0716-4	459	1520	3.42	9.27	149.6 ± 2.5	0.0550	3.4	0.1781	3.8	0.02347	1.7	0.441
0716-5	362	391	1.12	7.15	145.6 ± 2.6	0.0566	5.1	0.1784	5.4	0.02285	1.8	0.333
0716-6	189	182	0.99	3.69	143.5 ± 2.9	0.0555	5.2	0.1724	5.6	0.02252	2.0	0.365
0716-7	341	421	1.27	6.57	141.7 ± 2.5	0.0506	5.1	0.1552	5.4	0.02222	1.8	0.329
0716-8	1301	652	0.52	25.8	146.9 ± 2.7	0.0514	2.4	0.1634	3.1	0.02305	1.9	0.611
0716-9	353	306	0.90	7.16	149.9 ± 2.8	0.0545	3.5	0.1768	3.9	0.02353	1.9	0.476
0716-10	1382	784	0.59	26.3	140.7 ± 2.3	0.0535	3.0	0.1627	3.4	0.02207	1.7	0.485
0716-11	432	358	0.86	9.02	154.4 ± 2.6	0.0559	2.8	0.1867	3.3	0.02424	1.7	0.525
0716-12	172	229	1.37	3.49	147.5 ± 2.9	0.0500	11	0.160	11	0.02315	2.0	0.181

Errors are 1-sigma; Pb* indicate the radiogenic portions, respectively. Common Pb corrected using measured ^{204}Pb.

dikes often underwent moderate chloritization. The dikes were dated to be 148 ± 8 Ma by SHRIMP zircon U/Pb method (Bao et al., 2009b). The mafic dikes are of alkalic with 1.63–2.96% Na_2O and 1.15–3.67% K_2O, and relatively enriched in LILEs and have low whole-rock $\varepsilon_{Nd}(t)$ (−6.6 to −7.0) and zircon $\varepsilon_{Hf}(t)$ (−15.2 to −34.4) values, indicating that they may have been derived from an enriched mantle source (our unpublished data).

2.2. Heyu granite batholith

The Heyu granite batholith is exposed in an area of ~784 km^2 and is the largest Mesozoic granitic batholith in this region. It intruded the metamorphic rocks of the Taihua Group and the volcanic rocks of the Xiong'er Group. The batholith is a ring-like complex composed mainly of biotite monzogranite. The batholith was considered to have formed

Table 4
LA-ICPMS zircon U–Pb ages of the Heyu granite batholith.

Test no.	Pb* (ppm)	Th (ppm)	U (ppm)	Th/U	$^{207}Pb/^{206}Pb \pm 1\sigma$	$^{207}Pb/^{235}U \pm 1\sigma$	$^{206}Pb/^{238}U \pm 1\sigma$	$^{207}Pb/^{235}U \pm 1\sigma$ (Ma)	$^{206}Pb/^{238}U \pm 1\sigma$ (Ma)
Medium grained biotite monzogranite (Stage I)									
HY-14-01	46.92	132.5	269.5	0.49	0.08156 ± 215	1.46569 ± 3498	0.13034 ± 146	916 ± 14	790 ± 8
HY-14-02	31.83	1675	1009	1.66	0.11111 ± 135	0.34823 ± 387	0.02273 ± 24	303 ± 3	145 ± 2
HY-14-03	26.68	647.9	843.1	0.77	0.05356 ± 234	0.16701 ± 703	0.02262 ± 27	157 ± 6	144 ± 2
HY-14-04	24.54	535.9	782.1	0.69	0.05302 ± 199	0.18147 ± 650	0.02482 ± 28	169 ± 6	158 ± 2
HY-14-05	28.70	497.3	991.0	0.50	0.05258 ± 186	0.16319 ± 545	0.02251 ± 26	153 ± 5	143 ± 2
HY-14-06	57.86	100.1	171.6	0.58	0.09673 ± 254	3.13745 ± 7406	0.23525 ± 269	1442 ± 18	1362 ± 14
HY-14-07	31.94	675.9	856.0	0.79	0.06922 ± 364	0.21026 ± 1073	0.02203 ± 28	194 ± 9	140 ± 2
HY-14-08	15.86	283.3	462.9	0.61	0.05691 ± 321	0.18600 ± 1020	0.02370 ± 31	173 ± 9	151 ± 2
HY-14-09	36.47	495.1	1035	0.48	0.06639 ± 291	0.20858 ± 877	0.02279 ± 29	192 ± 7	145 ± 2
HY-14-10	37.77	1036	1113	0.93	0.08417 ± 347	0.26516 ± 1037	0.02285 ± 30	239 ± 8	146 ± 2
HY-14-11	32.70	652.1	1016	0.64	0.05533 ± 300	0.17949 ± 943	0.02353 ± 32	168 ± 8	150 ± 2
HY-14-12	31.81	799.7	913.1	0.88	0.05255 ± 294	0.16437 ± 895	0.02268 ± 29	155 ± 8	145 ± 2
HY-14-13	30.19	555.6	935.2	0.59	0.05542 ± 236	0.18035 ± 737	0.02360 ± 28	168 ± 6	150 ± 2
HY-14-14	29.46	612.3	977.7	0.63	0.05079 ± 208	0.16412 ± 644	0.02344 ± 28	154 ± 6	149 ± 2
HY-14-15	99.00	96.6	402.2	0.24	0.12761 ± 182	3.19570 ± 3208	0.18163 ± 184	1456 ± 8	1076 ± 10
HY-14-16	19.45	614.1	538.3	1.14	0.10926 ± 255	0.35019 ± 742	0.02324 ± 32	305 ± 6	148 ± 2
HY-14-17	24.49	624.4	662.4	0.94	0.07033 ± 335	0.22173 ± 1018	0.02287 ± 29	203 ± 8	146 ± 2
HY-14-18	35.80	567.8	879.1	0.65	0.05917 ± 343	0.19174 ± 1086	0.02350 ± 30	178 ± 9	150 ± 2
HY-14-19	34.12	833.1	991.4	0.84	0.05688 ± 267	0.18046 ± 817	0.02301 ± 28	168 ± 7	147 ± 2
HY-14-20	28.13	584.6	813.4	0.72	0.05016 ± 266	0.15904 ± 822	0.02299 ± 28	150 ± 7	147 ± 2
Coarse-grained biotite monzogranite (Stage II)									
HY-4-01	15.85	434.5	710.2	0.61	0.05017 ± 246	0.14496 ± 689	0.02096 ± 25	137 ± 6	134 ± 2
HY-4-03	35.56	1116	1375	0.81	0.05509 ± 726	0.17119 ± 2185	0.02254 ± 75	160 ± 19	144 ± 5
HY-4-04	8.52	276.7	295.5	0.94	0.05967 ± 277	0.20228 ± 1233	0.02449 ± 54	187 ± 10	156 ± 3
HY-4-05	27.32	718.9	1236	0.58	0.04741 ± 111	0.13391 ± 441	0.02073 ± 32	128 ± 4	132 ± 2
HY-4-06	17.68	692.9	684.2	1.01	0.06302165	0.17595 ± 675	0.02042 ± 24	165 ± 6	130 ± 2
HY-4-07	21.14	588.9	640.7	0.92	0.06498 ± 596	0.21160 ± 1908	0.02362 ± 40	195 ± 16	150 ± 3
HY-4-09	11.68	310.6	464.7	0.67	0.06953 ± 238	0.22457 ± 890	0.02381 ± 73	206 ± 7	152 ± 5
HY-4-11	21.16	541.2	845.1	0.64	0.05056 ± 101	0.16327 ± 465	0.02385 ± 61	154 ± 4	152 ± 4
HY-4-12	31.30	735.8	1292	0.57	0.05849 ± 88	0.18509 ± 503	0.02296 ± 48	172 ± 4	146 ± 3
HY-4-13	18.52	372.2	781.5	0.48	0.04832 ± 125	0.14380 ± 405	0.02192 ± 39	136 ± 4	140 ± 2
HY-4-16	172.9	405.5	782.2	0.52	0.08921 ± 191	2.38813 ± 4456	0.19416 ± 202	1239 ± 13	1144 ± 11
HY-4-18	16.22	544.5	744.0	0.73	0.04935 ± 95	0.13453 ± 256	0.01996 ± 13	128 ± 2	128 ± 0.8
HY-4-20	8.47	181.2	447.3	0.41	0.05111 ± 215	0.15421 ± 677	0.02194 ± 25	146 ± 6	140 ± 2
HY-4-22	22.97	770.8	946.0	0.81	0.05144 ± 95	0.14344 ± 497	0.02040 ± 48	136 ± 4	130 ± 3
HY-4-23	8.22	268.8	385.4	0.7	0.04882 ± 152	0.14085 ± 480	0.02115 ± 35	134 ± 4	135 ± 2
HY-4-24	74.95	297.4	378.7	0.79	0.08015 ± 305	1.87139 ± 6525	0.16934 ± 258	1071 ± 23	1008 ± 14
HY-4-25	31.65	910.5	1405	0.65	0.0573 ± 126	0.17821 ± 467	0.02305 ± 60	167 ± 4	147 ± 4
Fine-grained syenogranite dike									
HY-73-01	51.47	2201	845.9	0.38	0.19513 ± 1227	0.70326 ± 4098	0.02614 ± 62	541 ± 24	166 ± 4
HY-73-02	9.54	436.5	227.4	0.52	0.07347 ± 490	0.26838 ± 1729	0.02647 ± 54	241 ± 14	168 ± 3
HY-73-03	37.53	934.8	756.4	0.81	0.08606 ± 915	0.26458 ± 2754	0.02230 ± 48	238 ± 22	142 ± 3
HY-73-04	29.71	1595	964.2	0.6	0.06598 ± 157	0.19522 ± 441	0.02144 ± 27	181 ± 4	137 ± 2
HY-73-05	18.56	497.7	658.0	1.32	0.07731 ± 207	0.23923 ± 603	0.02242 ± 30	218 ± 5	143 ± 2
HY-73-06	63.34	15,196	14,748	0.97	0.09203 ± 627	0.25878 ± 1713	0.02039 ± 33	234 ± 14	130 ± 2
HY-73-07	41.96	890.4	1009	1.13	0.09480 ± 616	0.30493 ± 1909	0.02333 ± 41	270 ± 15	149 ± 3
HY-73-08	146.8	295.0	1042	3.53	0.08668 ± 200	1.3041 ± 2613	0.10911 ± 124	848 ± 12	668 ± 7
HY-73-09	26.00	994.5	946.4	0.95	0.06807 ± 160	0.20136 ± 449	0.02144 ± 27	186 ± 4	137 ± 2
HY-73-10	21.71	830.6	704.6	0.85	0.08938 ± 435	0.25975 ± 1198	0.02108 ± 33	234 ± 10	134 ± 2
HY-73-11	33.53	1477	997.3	0.68	0.09870 ± 209	0.31101 ± 608	0.02284 ± 29	275 ± 5	146 ± 2
HY-73-12	23.88	538.9	1011	1.88	0.05953 ± 154	0.17805 ± 438	0.02168 ± 28	166 ± 4	138 ± 2
HY-73-13	26.33	614.2	771.8	1.26	0.07814 ± 451	0.24128 ± 1341	0.02239 ± 35	219 ± 11	143 ± 2
HY-73-14	21.26	758.5	516.9	0.68	0.06543 ± 197	0.21018 ± 603	0.02329 ± 32	194 ± 5	148 ± 2
HY-73-15	28.62	1044	954.3	0.91	0.07647 ± 236	0.23556 ± 688	0.02234 ± 32	215 ± 6	142 ± 2
HY-73-16	12.04	317.5	142.7	0.45	0.06863 ± 462	0.29253 ± 1891	0.03091 ± 68	261 ± 15	196 ± 4
HY-73-17	29.53	1026	1012	0.99	0.07746 ± 156	0.23385 ± 441	0.02189 ± 27	213 ± 4	140 ± 2
HY-73-18	155.1	1457	1315	0.9	0.10255 ± 129	1.30589 ± 1520	0.09235 ± 103	848 ± 7	569 ± 6
HY-73-19	19.16	486.9	781.8	1.61	0.05754 ± 170	0.16802 ± 475	0.02118 ± 28	158 ± 4	135 ± 2
HY-73-20	11.84	451.9	348.1	0.77	0.08979 ± 667	0.29126 ± 2088	0.02353 ± 46	260 ± 16	150 ± 3

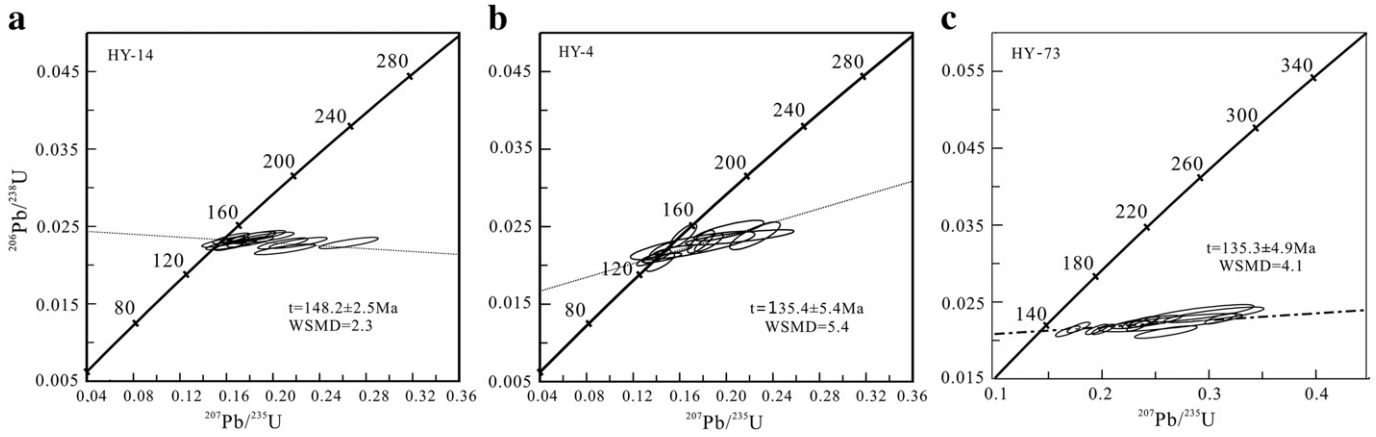

Fig. 5. Concordia plots of the zircons from the Heyu granite batholith.

by four to six phases of magma emplacement (Gao et al., 2010; Guo et al., 2009; Li et al., 2012c). Zircon U/Pb ages of the different stages vary from 148 ± 3 Ma to 134 ± 1 Ma (Gao et al., 2010; Guo et al., 2009; Li et al., 2012c, 2013a,b). However, based on the field relationship and our zircon U/Pb dating data we consider that the Heyu batholith emplaced in two major stages, ~148 ± 3 Ma and ~135 ± 5 Ma. Stage I (~148 Ma) medium-grained biotite monzogranite occurs in the center of the batholith and is capped with the rhyolite and andesite of the Paleoproterozoic volcanic rocks of the Xiong'er Group. The rocks in Stage I consist of 1–15% phenocryst and ~86% groundmass composed of perthite, plagioclase, quartz and biotite. Euhedral orthoclase and perthite are major phenocrysts and range in size from 0.8 × 1.0 cm to 1.5 × 2.5 cm. Accessory minerals include apatite, sphene and magnetite. Stage II (~135 Ma) coarse-grained to pegmatitic biotite monzogranite occurs in the margin of the batholith and makes up the major part of the batholith. The rocks in Stage II contain 20–40% phenocryst with a maximum of 60% in local places. Phenocryst is mainly K-feldspar ranging in size from 4 × 6 cm to 8 × 12 cm. The batholith is intruded by small-sized stocks or dikes of fine-grained biotite monzogranite, quartz syenite and biotite syenogranite. The stocks/dikes have similar ages to the rocks in Stage II. The batholith is shelled by a ~1–30 m-wide contact metamorphic zone, which consists mainly of biotite hornfels, biotite calcite–silicate hornfels, hornfelsed andesite and biotitized rhyolite.

One of the late-stage stocks that intruded the Heyu batholith is discovered to host the large Yuchiling porphyry Mo deposit with reserves of about 0.55 mt Mo metal at an average grade of 0.06% Mo (Li et al., 2013a,b; Zhou et al., 2009). The porphyry was obtained a weighted mean $^{206}Pb/^{238}U$ age of 134 ± 1 Ma using LA-ICP-MS zircon U/Pb dating method (Li et al., 2013a,b). Molybdenites from the ores yield an Re–Os isochron age of 131 ± 1 Ma (Zhou et al., 2009). The Yuchiling Mo deposit will not be discussed in this study because it occurs in the interior of the Heyu batholith, and far away from the Luanchuan Mo ore field.

3. Analytical results

3.1. Zircon U/Pb ages

Zircons from three Mo-bearing granites in the Luanchuan ore field are clear, colorless, euhedral crystals, and range in size from 50 to 100 >μm. Most zircon grains show oscillatory zoning in CL images but a few grains have inherited cores (Fig. 3).

Zircons from the Nannihu granite porphyry have 578 to 2553 ppm Th and 802 to 3950 ppm U, with Th/U ratios varying from 0.05 to 1.07 (Table 1). Most zircon grains have Th/U ratios ranging from 0.4 to 0.8, typical of magmatic origin (Corfu et al., 2003). Twenty of the 35 analyzed spots yield a weighted mean $^{206}Pb/^{238}U$ age of 149.6 ± 0.4 Ma (MSWD = 1.5), which is interpreted as the crystallization age of the Nannihu granite porphyry (Fig. 4a). One grain (LN-3.26) contains high radiogenic Pb (1174 ppm) and $^{206}Pb/^{238}U$ age of 1534 ± 7 Ma, which may be inherited from Mesoproterozoic source rocks or entrapment from earlier igneous rocks during magma segregation and ascent. Another grain (LN-3.10) has a $^{206}Pb/^{238}U$ age of 168 ± 1 Ma, likely an entrapment during the ascent of magmas.

Zircons from the Shangfanggou granite porphyry contain highly radiogenic Pb (47 to 606 ppm), Th (346 to 2155 ppm) and U (774 to 6226 ppm), with Th/U ratios ranging from 0.29 to 1.3 (Table 2). Twenty-nine analyzed spots give a weighted mean $^{206}Pb/^{238}U$ age of 135.4 ± 0.3 Ma (MSWD = 1.4) (Fig. 4b).

Zircons from the Shibaogou granite porphyry have Th/U ratios ranging from 0.30 to 1.12, and yield a weighted mean $^{206}Pb/^{238}U$ age of 147.2 ± 1.7 Ma (MSWD = 0.85). Zircons from the late-stage, fine-grained syenogranite have Th/U ratios of 0.52–3.42, and a weighted mean $^{206}Pb/^{238}U$ age of 145.3 ± 1.7 Ma (MSWD = 1.6) (Table 3) (Fig. 4c and d).

Zircons from the Heyu granite batholith are colorless to yellowish euhedral prism crystals, ranging in size from ~80 to ~150 μm. Most zircons show clear oscillatory zoning in CL images and only a few of them contain inherited cores (Fig. 3). Zircons have Th/U ratios varying from 0.38 to 3.53, typical of magmatic zircon. Twenty spots on the zircons from Stage I biotite monzogranite (HY-14) have $^{206}Pb/^{238}U$ ages varying from 140 Ma to 150 Ma. Three grains (HY14-01, HY-14-06 and HY-14-15) have $^{206}Pb/^{238}U$ ages of 790 Ma, 1362 Ma and 1076 Ma, respectively, likely inherited zircons. The other three spots shift away from the concordia. A total of 14 grains yield a U–Pb concordia age of 148.2 ± 2.5 Ma (MSWD = 2.3, Table 4, Fig. 5a). Fifteen grains from Stage II biotite monzogranite (HY-4) give a concordia age of 135.4 ± 5.4 Ma (MSWD = 3.8) (Table 4 and Fig. 5b). Two spots (HY-4-16 and HY-4-24) have $^{206}Pb/^{238}U$ ages of 1144 Ma and 1008 Ma in old cores. Fifteen spots from the syenogranite dike (HY-73) give a concordia U–Pb age of 135.3 ± 4.9 Ma (MSWD = 4.1) (Table 4 and Fig. 5c), indicating that the syenogranite dike is coeval to Stage II biotite monzogranite.

3.2. Major and trace elements

Rocks from the Nannihu, Shangfanggou and Shibaogou granite porphyries have high SiO_2 varying from 72.1 to 79.1 wt.% (Table 5). They are enriched in K_2O and plot in the high-K to shoshonitic field in the plot of SiO_2 versus K_2O (Fig. 6a). On the plot of SiO_2 versus $K_2O + Na_2O$–CaO, most of them plot in both alkalic–calcic and alkalic fields (Fig. 6b). The Heyu granite batholith has SiO_2 varying from 67.2 to 75.4 wt.%, lower than those of the granite porphyries in the Luanchuan ore field (Fig. 6).

Table 5
Major and trace element compositions of the granites in the study area (wt.% for major elements and ppm for trace elements).

	Nannihu granite porphyry				Shangfanggou granite porphyry		Shibaogou granite porphyry				Heyu medium-grained biotite monzogranite (Stage I)							
	LN-1	LN-2	LN-3	LN-4	LS-6	LS-9	07-13	07-14	07-15	07-16	HY-10	HY-14	HY-16	HY-19	HY-33	HY-41	HY-43	HY-44
SiO_2	76.06	74.12	76.97	73.94	77.09	79.13	72.06	73.79	73.43	74.86	69.37	69.6	67.16	67.33	75.27	71.63	72.91	71.35
TiO_2	0.19	0.21	0.09	0.18	0.09	0.09	0.14	0.12	0.18	0.08	0.35	0.32	0.51	0.56	0.22	0.18	0.25	0.27
Al_2O_3	12.59	12.87	12.92	14.06	12.64	11.38	15.03	14.16	14.46	13.49	15.71	15.3	15.9	15.92	13.29	15.54	14.39	14.97
$Fe_2O_3^T$	0.96	1.30	0.93	2.25	0.68	0.97	1.08	1.08	1.42	0.11	2.82	2.07	3.85	4.19	1.69	1.53	1.95	2.12
MnO	0.00	0.00	0.01	0.01	0.01	0.01	0.04	0.03	0.06	0.03	0.05	0.05	0.09	0.12	0.04	0.04	0.04	0.03
MgO	0.16	0.15	0.28	0.19	0.05	0.18	0.30	0.17	0.38	0.22	0.74	0.52	1.02	1.12	0.49	0.38	0.45	0.45
CaO	0.01	0.01	0.10	0.45	0.01	0.38	1.35	0.95	1.42	1.43	1.55	1.50	2.52	1.77	1.18	1.05	1.09	1.17
Na_2O	1.87	1.67	2.33	1.86	1.37	2.26	4.00	4.24	3.97	3.68	4.79	4.23	4.90	4.99	4.00	4.55	3.96	4.99
K_2O	7.30	7.99	6.11	6.63	7.89	5.02	5.15	4.87	4.31	4.92	4.31	4.77	3.66	3.5	3.77	5.00	4.83	4.49
P_2O_5	0.03	0.04	0.00	0.03	0.00	0.02	0.06	0.03	0.07	0.01	0.19	0.15	0.24	0.32	0.07	0.05	0.10	0.09
LOI	0.63	1.13	0.70	0.99	0.54	0.67	0.45	0.50	0.35	0.97	1.71	1.17	0.3	1.62	0.61	0.86	1.01	1.49
Total	99.79	99.48	100.44	100.60	100.35	100.09	99.67	99.93	100.05	99.82	99.88	99.75	99.84	99.83	100.02	99.94	99.96	99.93
DI	96	95	95.7	93.5	97.1	96.3	96.5	97.5	96.1	97.5	93.6	93.6	92.2	89.9	96	96.3	95.5	96.2
ASI	1.14	1.13	1.21	1.27	1.17	1.16	1.03	1.01	1.05	0.96	1.02	1.03	0.96	1.05	1.04	1.05	1.05	0.98
Ga	20.8	26.1	20.5	27.6	19.3	21.4	20.8	21.9	23.8	21.6	20.8	25.1	22.3	26.0	19.8	20.7	19.8	18.3
Rb	337	295	351	436	249	197	212	237	242	168	60.9	176	49.5	33.4	117	109	75.0	61.8
Ba	942	217	904	830	122	81.4	1427	754	816	382	1842	2214	2195	1660	543	1778	1649	2088
Th	34.2	41.8	32.9	39.6	39.8	32.4	24.3	31.8	28.4	33.6	13.4	32.0	16.6	19.8	13.0	12.1	18.6	18.6
U	29.6	7.37	25.2	20.8	20.0	3.96	4.11	9.51	5.33	12.1	1.65	4.70	2.10	4.90	1.73	1.73	2.24	1.51
Nb	53.9	87.7	70.4	50.9	36.8	30.4	32.6	68.5	42.7	115	36.0	37.3	41.8	120	34.4	27.7	36.1	33.9
Ta	4.08	7.64	6.35	4.22	2.44	2.07	2.20	5.10	3.38	7.36	2.21	2.09	2.44	8.26	2.77	1.67	2.48	2.23
Sr	124	54.5	138	75.9	43.9	42.9	443	229	377	85.6	247	848	654	468	102	254	229	338
Y	9.71	6.27	9.04	14.6	7.25	3.73	7.79	16.6	9.69	25.8	10.4	15.1	15.4	17.3	6.10	3.21	6.60	5.43
Pb	25.8	13.4	17.5	43.3	14.3	18.8	27.0	18.3	27.4	14.8	8.51	19.4	13.0	20.3	10.3	12.9	11.6	11.4
Zr	143	123	152	136	75.3	68.7	97.3	133	106	93.6	139	118	119	129	124	86.4	95.1	90.0
Hf	4.99	6.84	6.23	4.52	3.46	2.92	3.20	4.23	3.57	4.16	3.43	2.45	2.90	3.92	4.16	2.66	2.57	2.07
La	43.6	16.9	48.4	72.9	10.9	11.2	30.4	33.6	34.8	6.51	36.4	69.1	61.4	44.9	15.6	13.6	34.1	28.7
Ce	71.5	26.8	81.5	118	23.2	19.7	48.5	57.7	57.6	17.1	58.8	122	102	92.3	26.3	30.1	54.9	51.5
Pr	7.16	2.61	8.02	11.7	2.63	1.91	4.83	5.96	5.88	2.45	6.56	11.8	11.9	11.3	3.19	3.26	6.57	5.68
Nd	22.1	7.20	24.3	34.5	8.26	5.19	14.8	18.5	18.4	8.96	22.1	39.2	40.3	41.9	11.3	11.4	21.7	18.9
Sm	3.25	1.03	3.42	5.02	1.21	0.686	1.81	2.49	2.34	1.67	3.30	5.63	6.36	7.41	1.88	1.86	3.30	2.81
Eu	0.540	0.210	0.552	0.660	0.200	0.128	0.580	0.511	0.567	0.192	0.840	1.19	1.42	1.52	0.38	0.44	0.69	0.630
Gd	2.03	0.723	2.11	3.56	0.879	0.544	1.66	2.42	2.12	1.73	2.40	3.46	4.24	4.80	1.33	1.22	2.12	1.84
Tb	0.287	0.119	0.277	0.435	0.136	0.067	0.206	0.349	0.252	0.354	0.330	0.500	0.590	0.700	0.200	0.170	0.290	0.260
Dy	1.44	0.761	1.53	2.19	0.871	0.430	1.05	2.14	1.39	2.56	1.69	2.35	2.80	3.42	0.970	0.790	1.44	1.27
Ho	0.272	0.155	0.279	0.396	0.178	0.093	0.224	0.470	0.282	0.642	0.320	0.420	0.510	0.690	0.190	0.140	0.270	0.250
Er	0.818	0.536	0.859	1.21	0.605	0.322	0.728	1.58	0.894	2.44	0.940	1.18	1.52	2.08	0.630	0.460	0.770	0.690
Tm	0.132	0.110	0.141	0.171	0.104	0.061	0.124	0.282	0.149	0.474	0.140	0.170	0.210	0.310	0.090	0.060	0.110	0.100
Yb	1.03	1.03	1.092	1.29	0.824	0.535	0.919	2.07	1.133	3.75	0.900	1.07	1.30	2.16	0.710	0.430	0.720	0.650
Lu	0.185	0.237	0.200	0.217	0.152	0.106	0.166	0.349	0.206	0.635	0.120	0.150	0.180	0.330	0.120	0.070	0.110	0.090
∑REE	154.4	58.4	172.7	252.2	50.2	41.0	106.0	128.4	126.0	49.5	134.8	258.2	234.7	213.8	62.9	64.0	127.1	113.4
$(La/Yb)_N$	30.4	11.8	31.8	40.7	9.48	15.0	23.7	11.7	22.1	1.24	29.0	46.3	33.9	14.9	15.8	22.7	34.0	31.7
Eu/Eu*	0.64	0.74	0.63	0.48	0.59	0.64	1.02	0.64	0.78	0.35	0.91	0.82	0.84	0.78	0.73	0.89	0.80	0.85
T_{Zr} (°C)	831	814	840	830	775	768	786	815	796	782	816	801	795	808	811	777	786	777

	Heyu coarse-grained biotite monzogranite (Stage II)							Heyu fine-grained monzogranite and syenogranite (dikes)										
	HY-22	HY-34	HY-38	HY-39	HY-40	HY-59	HY-60	HY-24	HY-28	HY-31	HY-42	HY-45	HY-57	HY-48	HY-50	HY-51	HY-52	HY-53
SiO_2	72.68	73.64	72.73	71.79	72.53	70.67	69.78	72	71.8	72.37	71.62	71.07	73.28	74.77	71.86	72.65	71.82	75.43
TiO_2	0.35	0.25	0.31	0.25	0.29	0.30	0.38	0.28	0.31	0.29	0.25	0.32	0.23	0.15	0.21	0.23	0.21	0.13
Al_2O_3	14.39	13.71	14	14.85	14.34	15.15	15.22	14.81	14.81	14.64	15.04	14.98	14.36	13.77	15	14.45	15.11	13.74
$Fe_2O_3^T$	2.74	2.11	2.56	2.02	2.30	2.23	2.62	2.37	2.21	2.04	2.22	2.66	2.08	1.49	2.20	1.91	2.15	1.38
MnO	0.06	0.06	0.06	0.05	0.04	0.04	0.06	0.04	0.05	0.04	0.07	0.06	0.04	0.03	0.06	0.05	0.06	0.02
MgO	0.79	0.62	0.56	0.47	0.45	0.54	0.62	0.66	0.71	0.63	0.56	0.58	0.42	0.27	0.37	0.39	0.38	0.26
CaO	1.59	1.4	1.67	1.26	1.44	1.42	1.67	1.32	1.56	1.4	0.94	1.39	1.33	1.03	1.13	1.16	0.92	0.79
Na_2O	3.99	3.99	4.53	4.43	4.51	4.82	4.44	3.89	4.18	4.04	4.49	4.42	4.00	4.12	4.40	4.70	4.64	4.13
K_2O	3.65	4.12	3.43	4.73	3.95	4.62	4.94	4.44	4.19	4.41	4.66	4.32	4.15	4.37	4.63	4.37	4.56	4.11
P_2O_5	0.15	0.09	0.12	0.09	0.12	0.14	0.16	0.11	0.11	0.1	0.09	0.12	0.08	0.04	0.07	0.07	0.07	0.03
LOI	0.61	0.6	0.69	0.6	0.84	0.67	0.6	0.64	0.49	0.41	0.74	0.61	0.61	0.44	0.53	0.5	0.52	0.57
Total	99.96	99.98	99.97	99.94	99.96	99.92	99.89	99.93	99.94	99.95	99.93	99.91	99.97	100.01	99.93	99.96	99.93	100.02
DI	93.6	95.5	96.3	95.9	95.6	95.7	94.8	93.9	94.5	94.9	94.7	94.4	95.3	97.1	95.5	96.6	95.4	96.6
ASI	1.07	1.01	0.98	1.01	1.00	0.98	0.97	1.09	1.04	1.05	1.06	1.03	1.06	1.03	1.05	0.99	1.06	1.08
Ga	19.3	19.3	22.8	21.3	21.7	22.3	21.4	20.7	19.8	19.6	20.4	22.0	20.5	20.4	21.7	19.6	21.4	19.9
Rb	88.7	102	82.7	110	108	154	87.6	94.5	69.2	77.1	89.8	79.6	69.0	103	98.0	97.2	109	116
Ba	545	544	1030	1949	1242	1895	2131	1585	1114	1178	1724	1821	1735	909	1885	1317	1981	594
Th	19.5	16.5	29.9	20.8	25.9	31.2	19.8	12.1	10.8	10.7	15.2	23.8	10.8	16.7	17.0	10.4	13.9	17.4
U	2.24	2.17	6.53	3.87	3.98	46.0	4.06	1.83	1.82	1.91	2.42	2.08	1.18	2.88	1.62	1.95	1.77	4.98
Nb	31.1	29.9	47.5	36.9	45.9	33.8	39.7	24.2	27.2	26.1	34.0	45.7	32.5	26.8	40.3	37.7	35.5	37.0
Ta	2.28	2.34	3.09	2.35	3.00	1.90	2.27	1.66	2.19	2.05	1.96	3.21	2.12	1.81	2.34	2.39	2.27	3.32
Sr	168	133	371	402	286	657	507	264	211	208	322	349	193	138	358	152	316	120
Y	9.29	6.34	7.46	5.07	6.94	9.57	7.57	8.81	7.00	4.95	5.85	13.3	7.47	3.97	8.95	7.30	5.38	4.63
Pb	9.96	13.9	12.0	10.4	11.4	18.1	15.5	13.9	13.6	12.2	13.6	24.3	14.2	16.9	15.6	17.9	16.27	18.8
Zr	127	110	116	97.6	126	143	143	101	98.3	96.0	91.5	126	132	64.2	73.1	92.3	88.5	96.8
Hf	3.96	3.84	3.79	3.05	3.98	3.79	3.44	3.21	3.14	3.30	2.42	3.21	3.34	1.80	2.15	2.35	2.36	3.07
La	25.1	15.4	38.4	25.0	34.3	55.6	38.4	23.3	19.4	17.2	32.4	55.5	27.0	19.5	37.4	25.5	32.3	14.0
Ce	38.2	29.2	77.9	46.8	61.3	96.8	72	43.5	34.2	32.6	57.1	105.0	43.9	35.6	72.6	41.2	61.3	26.8
Pr	4.87	3.21	7.64	5.45	7.37	9.69	8.12	5.19	4.20	4.06	6.46	11.7	5.45	4.05	8.23	4.97	6.81	2.92
Nd	17.1	11.4	25.6	19.0	25.0	31.3	28.1	18.9	15.2	14.6	21.6	39.1	18.0	13.2	28.4	16.7	22.5	9.53
Sm	2.94	2.02	3.84	2.82	3.81	4.47	4.25	3.10	2.62	2.54	3.08	5.58	2.83	2.00	4.41	2.58	3.33	1.63
Eu	0.610	0.440	0.820	0.690	0.790	1.11	0.98	0.800	0.610	0.530	0.680	0.970	0.590	0.370	0.940	0.460	0.630	0.260
Gd	2.06	1.40	2.64	1.79	2.30	2.79	2.62	2.19	1.83	1.70	2.04	3.48	1.79	1.31	2.74	1.72	2.03	1.05
Tb	0.310	0.200	0.340	0.260	0.350	0.390	0.370	0.320	0.270	0.240	0.260	0.500	0.260	0.180	0.400	0.230	0.270	0.170
Dy	1.57	1.08	1.71	1.28	1.65	1.72	1.77	1.65	1.31	1.19	1.21	2.43	1.26	0.880	2.04	1.20	1.23	0.880
Ho	0.300	0.220	0.320	0.230	0.310	0.320	0.320	0.300	0.250	0.230	0.220	0.510	0.240	0.160	0.390	0.240	0.210	0.180
Er	0.920	0.640	0.970	0.700	0.9	0.87	0.93	0.860	0.720	0.610	0.680	1.56	0.740	0.460	1.10	0.740	0.620	0.540
Tm	0.130	0.100	0.130	0.100	0.12	0.12	0.12	0.140	0.110	0.080	0.080	0.240	0.100	0.060	0.150	0.100	0.080	0.080
Yb	0.960	0.760	0.920	0.660	0.850	0.800	0.780	0.860	0.710	0.580	0.570	1.73	0.680	0.450	0.980	0.750	0.550	0.610
Lu	0.130	0.130	0.130	0.110	0.130	0.120	0.110	0.130	0.100	0.080	0.080	0.270	0.110	0.060	0.140	0.120	0.080	0.090
$\sum$REE	95.2	66.2	161.4	104.9	139.2	216.1	158.9	101.2	81.5	76.2	126.5	228.6	102.9	78.3	159.9	96.5	131.9	58.7
$(La/Yb)_N$	18.8	14.5	29.9	27.2	29.0	49.9	35.3	19.4	19.6	21.3	40.8	23.0	28.5	31.1	27.4	24.4	42.1	16.5
Eu/Eu*	0.76	0.80	0.79	0.94	0.75	0.89	0.83	0.94	0.85	0.78	0.83	0.67	0.80	0.70	0.83	0.67	0.74	0.61
T_{Zr} (°C)	813	798	800	785	808	816	815	793	788	787	783	809	817	754	763	780	780	792

The granite porphyries in the Luanchuan ore field have high differentiation index (DI) ranging from 89.9 to 97.5 and aluminum saturation index (ASI) from 0.96 to 1.27, consistent with metaluminous to peraluminous. The Heyu granite batholith has DI and ASI lower than those of the granite porphyries in the Luanchuan ore field. The rocks from the Luanchuan ore field and the Heyu batholith have DI and ASI indices and K_2O increasing with increasing SiO_2, and Al_2O_3, TiO_2, $Fe_2O_3^{total}$ and P_2O_5 decreasing with increasing SiO_2 (Fig. 7). All the rocks have Sr, Ba and total REE decreasing with increasing SiO_2, and Rb/Sr ratios increasing with increasing SiO_2 (Fig. 8). The correlations of the elements are consistent with crystal fractionation of ferromagnesian minerals, Fe–Ti oxides, plagioclase and apatite during the formation of the rocks. All the rocks have positive correlations between Sm and Nd and between Nb and Ta (Fig. 8d and e). The rocks show an I-type trend of differentiation on the plots of P_2O_5 versus SiO_2 and Th versus Rb (Figs. 7d and 8f).

Samples from the granite porphyries in the Luanchuan ore field and the Heyu granite batholith have bulk REE concentrations ranging from 41 to 258 ppm with the $(La/Yb)_N$ ratios varying from 9.48 to 49.9. They show right dipping profiles with negative Eu anomalies on the chondrite-normalized REE patterns (Fig. 9a–f). The granite porphyries are relatively depleted in middle REE and show concave profiles, consistent with high degrees of differentiation. All the rocks exhibit strong negative Ba, Sr, P and Ti anomalies on the primitive mantle-normalized trace element patterns (Fig. 10).

Zircon saturation temperature of the granitic magma is estimated to be 750 to 840 °C (Table 5) using zircon saturation thermometer (Watson and Harrison, 1983). Given most zircons are of magmatic in origin, the temperature can be interpreted as the minimum magma temperature, which is consistent with the homogenization temperature (920 to 950 °C) of the melt inclusions in the quartz phenocryst of the Nannihu granite porphyry (Hu et al., 1988).

3.3. Rare earth elements of zircons from the Nannihu granite porphyry

Zircons from the Nannihu granite porphyry show heavy REE-enriched patterns with significant positive Ce anomalies and weakly negative Eu anomalies on the chondrite-normalized REE patterns (Fig. 11). Zircons have Ce^{4+}/Ce^{3+} ratios varying from 53 to 278 with an average value of 120, and Ce anomalies of 1.6 to 28.4 (Table 6), typical of zircons from unaltered igneous rocks (Hoskin and Schaltegger, 2003).

3.4. Whole-rock Nd isotopic compositions

Samples from the granite porphyries in the Luanchuan ore field and the Heyu granite batholith have similar Sm–Nd isotopic compositions. They have $^{143}Nd/^{144}Nd$ ratios ranging from 0.511646 to 0.512217 and $\varepsilon_{Nd}(t)$ values from −11.3 to −17.5. $f_{Sm/Nd}$ ratios are estimated to be −0.41 to −0.62. One-stage Nd model ages vary from 1.4 to 2.1 Ga and two-stage Nd model ages [$T_{DM2}(Nd)$] from 1.7 to 2.5 Ga (Table 7).

3.5. Zircon Lu–Hf isotopic compositions

Zircons from the granite porphyries in the Luanchuan ore field have Lu–Hf isotopic compositions similar to those from the Heyu granite batholith (Table 8). The calculated one-stage Hf model ages [$T_{DM1}(Hf)$] vary from 1.1 to 2.5 Ga and two-stage Hf model ages [$T_{DM2}(Hf)$] from 1.6 to 3.4 Ga with most between 2.2 and 2.5 Ga (Fig. 12a). On the plot of zircon U/Pb age versus ε_{Hf} values, they plot in the similar range of $\varepsilon_{Hf}(t)$ values (−5.8 to −35.6). Almost all of the zircons have $\varepsilon_{Hf}(t)$ values above the 3.0-Ga crustal evolution line (Fig. 12b).

4. Discussions

4.1. A genetic link between granite porphyries in the Luanchuan ore field and the Heyu granite batholith

The granite porphyries in the Luanchuan ore field and the Heyu granite batholith have similar whole-rock major, trace element and Nd isotopic and zircon Hf isotopic compositions (Figs. 6–10 and 12), indicating that they may have been derived from similar source rocks. The Nannihu and Shibaogou granite porphyries have zircon U/Pb ages similar to Stage I biotite monzogranite of the Heyu granite batholith, indicating that they may have emplaced concurrently (Figs. 4a,5a), whereas the Shangfanggou granite porphyry is nearly coeval with Stage II biotite monzogranite of the Heyu granite batholith. Therefore, the granite porphyries in the Luanchuan ore field are temporally related to the Heyu granite batholith. In addition, regional geophysical data of gravity and magnetic anomalies show that the small granite porphyries in the Luanchuan ore field may be underlain by a huge granite body (about 40 × 25 km in size), which is likely connected with the Heyu batholith to the east (Wang et al., 2006; Xu et al., 2003a). This discovery indicates that the granite porphyries in the Luanchuan ore field and the Heyu granite batholith may be spatially associated at depth.

The Heyu granite batholith itself is intruded by a few proximately coeval granite porphyry stocks/dikes that host Mo deposits in the interior of the batholith. The granite porphyry stocks/dikes have compositions identical to Stage II biotite monzogranite of the Heyu batholith, indicating that the porphyry stocks/dikes are likely extrusive analogs of Stage II biotite monzogranite. It is likely that intensive uplifting and erosion in Mesozoic may have eroded the epithermal counterparts for the porphyry- and skarn-type mineralization in this region, instead those plutons at depth may have been exposed on the surface due to intensive uplift. We thus propose that the Heyu granite batholith is likely the precursor of the granite porphyries in the Luanchuan ore field. The Mo mineralization may have occurred through differentiation of the granitic magma and fluid–magma interactions in late stage. Differentiation and fluid (vapor) extraction of Mo from the Heyu granite batholith are responsible for the formation of porphyry- and skarn-type ore deposits in the East Qinling Mo mineralization belt.

4.2. Source rocks of the granitic rocks

Granite porphyries in the Luanchuan ore field and the Heyu granite batholith have $T_{DM2}(Nd)$ ages (1.7 to 2.5 Ga) and $T_{DM2}(Hf)$ ages (2.2 to 2.5 Ga) younger than the Archean Taihua Group, which has a crystallization age of ~2.7 Ga and $T_{DM2}(Hf)$ ages of 2.8 to 3.2 Ga (Diwu et al., 2010; Huang et al., 2010). Likewise, Mesozoic granites elsewhere in the East Qinling orogen also have $\varepsilon_{Nd}(t)$ and $\varepsilon_{Hf}(t)$ values similar to the granite porphyries in the Luanchuan ore field, and they have $T_{DM2}(Nd)$ ages ranging from 1.8 to 2.5 Ga (Guo et al., 2009; Wei et al., 2010; Yao et al., 2009), also younger than the Taihua Group. Nevertheless, unlike the granite porphyries in the Luanchuan ore field, Mesozoic granites elsewhere in the eastern part of the North China Craton have relatively restricted whole-rock $\varepsilon_{Nd}(t)$ and zircon $\varepsilon_{Hf}(t)$ values for individual plutons, and have older zircon $T_{DM2}(Hf)$ ages (2.5 to 2.7 Ga) and ubiquitously contain ~2.5 Ga inherited zircons (Jiang et al., 2013; Yang et al., 2013). Therefore, it is unlikely that the granite porphyries in the Luanchuan ore field formed from remelting of the Taihua Group (Chen et al., 2000; Lu et al., 2002; Yang et al., 2010).

Some researchers proposed that the Mesozoic granites in this region formed from a mixed source of remelts of the Taihua and the Xiong'er Groups and mantle-derived melts (e.g., Li et al., 2012c; Zhang et al., 2010; Zhu et al., 2010a). However, the Mesozoic granites have Nd and Hf isotopic compositions remarkably different from the Taihua and Xiong'er Groups. If the mafic dikes in the ore field (148 ± 2 Ma, SHRIMP zircon U–Pb method, Bao et al., 2009b) can be considered as the mantle end member (ε_{Nd}(147 Ma) = −6.6 to −7.0), then such

mantle component should be predominant in the magma source for the crust–mantle hypothesis. This mantle scenario is unlikely to be true for the peraluminous granites on major element grounds (Collins, 1998; Gray, 1984).

The basement of the Yangtze Block is younger than that of the North China Craton. Although a 3.8-Ga old detrital zircon was reported from the basement of the Yangtze Block (Zhang et al., 2006a), the basement is mainly composed of Paleoproterozoic rocks with T_{DM2}(Nd) ages ranging from 1.8 to 2.2 Ga (Chen et al., 1999; Li et al., 1994; Ling et al., 2008; Wang et al., 2013; Zhang and Zheng, 2007; Zhang et al., 1995, 1997). In addition, Neoproterozoic magmatic rocks occur widely in the periphery of the Yangtze Block and are considered to have derived from remelting of Archean and Paleoproterozoic crusts and remelts of juvenile crust (Zhang and Zheng, 2007). Granite porphyries in the Luanchuan ore field have two-stage Nd and Hf model ages ranging from 1.4 to 2.5 Ga, similar to T_{DM2}(Nd) ages of the basement of the Yangtze Block (Zhang et al., 2006b), indicating that the granite porphyries may have derived from remelting of subducted continental crust of the Yangtze Block. The presence of the inherited zircons in the Heyu batholith (Tables 1, 4) also indicates the involvement of the subducted Neoproterozoic magmatic rocks of the Yangtze Block (Huang et al., 2006). The Mesozoic granites in North Qinling and the southern margin of the North China Craton have low radiogenic Pb isotopic ratios. Feldspars commonly contain negligible U and Th so that the Pb isotopic compositions of feldspar can be considered as initial Pb isotopic ratios of the magmas. K-feldspars from the Mesozoic granites have Pb isotopic ratios of 15.91 to 18.12 $^{206}Pb/^{204}Pb$, 15.08 to 15.68 $^{207}Pb/^{204}Pb$ and 36.95 to 38.51 $^{208}Pb/^{204}Pb$, similar to the northern margin of the Yangtze Block rather than the North China Craton (Hu et al., 1988; Li et al., 2011; Zhang, 1988; Zhang and Wang, 1991; Zhang et al., 1987). Mesozoic granitic rocks in the Dabie and Sulu area also have low radiogenic Pb isotopic compositions, which are consistent with the involvement of the subducted crust in the northern margin of the Yangtze Block (Xu et al., 2009; Zhao and Zheng, 2009). Remelting of the subducted crust of the Yangtze Block may be attributed to upwelling asthenospheric mantle under post-collisional tectonic regime and underplating of basaltic magma derived from previously enriched mantle wedge.

Two-pyroxene granulite enclaves trapped in the Mesozoic granite porphyries in the East Qinling orogen indicate that the Mesozoic granite porphyries may have formed at depth of more than 30 km (Wang et al., 1986). It is reported that the lower crust and mantle enclaves occur in the ~160 Ma Xinyang diatremes in the southern margin of the North China Craton, indicating that the lower crust enclaves are derived from ~30–45 km depth (Zheng et al., 2008). The lower crust enclaves are composed of high-pressure mafic to felsic granulite and metagabbro with low radiogenic Pb isotopic composition, similar to that of the Yangtze Block (Lu et al., 2003). It is therefore proposed that the northward continental subduction of the Yangtze Block beneath the North China Craton at Triassic may have reached a depth of 200 km or more in Dabie–Sulu orogen (Zhang et al., 1996, 2009) and extended as far as 400 km laterally (Lu et al., 2003). New geophysical results show that the lower crust beneath the southern margin of the North China Craton is thin, and the Moho dips northward, the imaged high-velocity volumes in the intralithospheric mantle beneath the southern margin of the North China Craton was interpreted to be a subduction remnant that still exists in the uppermost mantle, which reveal a flat subduction of the Yangtze Block beneath the North China Craton (Zheng et al., 2012a). Therefore, it is likely that the stagnant subducted continental crust of the Yangtze Block may have existed at the depth of the lower crust in the southern margin of North China Craton in Mesozoic (Lu et al., 2003, 2004; Zheng et al., 2008, 2009).

Previous studies on continental orogens indicate that slices of silica-rich continental crust that subducted into the mantle during collision may have undergone metamorphism and exhumation as coherent high-pressure or ultrahigh-pressure (HP or UHP) terranes or, if stalled in the mantle, melting and return towards the surface as magmas, or a

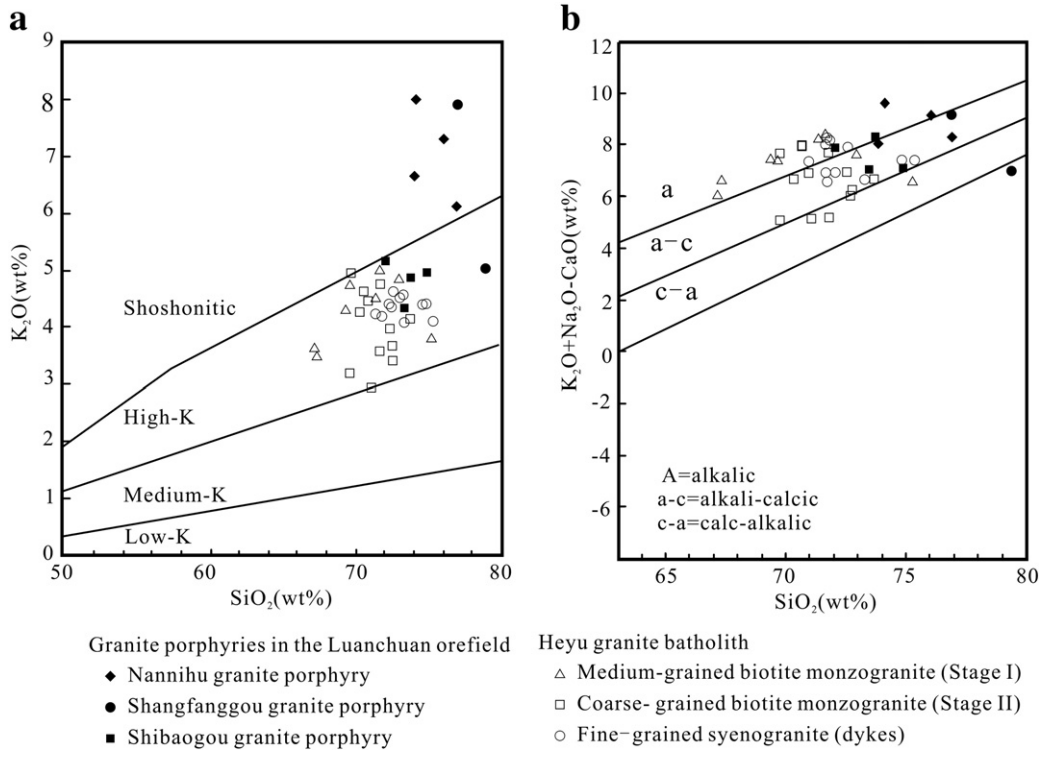

Fig. 6. Plots of SiO_2 vs. K_2O (a) and $K_2O + Na_2O$–CaO (b) for the granite porphyries in the Luanchuan ore field and the Heyu granite batholith. Reference lines after Frost et al. (2001).

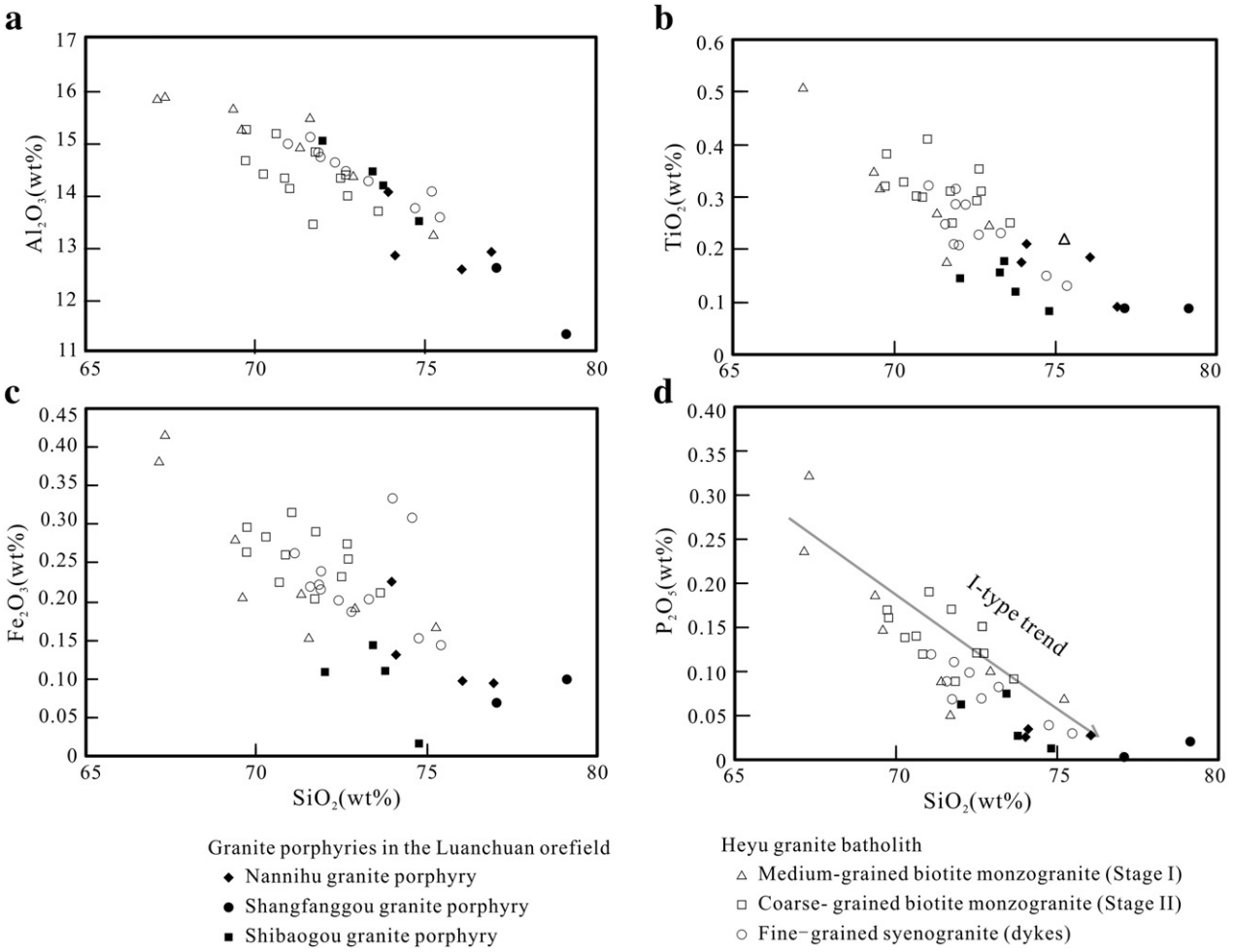

Fig. 7. Variations of Al_2O_3 (a), TiO_2 (b), FeO^{total} (c), and P_2O_5 (d) against SiO_2 for the granite porphyries in the Luanchuan ore field and the Heyu granite batholith.

combination of these two processes (Brueckner, 2009). Large-scale, collisional UHP terranes routinely stall at the continental Moho where diminishing body forces are exceeded by boundary forces (Walsh and Hacker, 2004). We therefore propose that the granite porphyry in the Luanchuan ore field and elsewhere in the East Qinling orogen were derived from remelting of the subducted crust of the Yangtze Block during the transition of regional tectonic regime from subduction to post-collisional extension (Mao et al., 2008).

4.3. Implications for the source of Mo of the East Qinling Mo mineralization belt

Porphyry Cu and Cu–Mo deposits are generally related to oxidized magma such as adakite, whereas Mo mineralization is commonly associated with less oxidized magma which formed from remelting of continental crust (Candela and Bouton, 1990; Oyarzun et al., 2002; Vigneresse, 2007). Zircons from porphyry bodies related to Cu mineralization in the northern Chile and the Tibetan area of China have an averaged Ce^{4+}/Ce^{3+} ratio higher than 200, indicating highly oxidized conditions of magmas (Ballard et al., 2002; Liang et al., 2006). Zircons from the granite porphyries related to Mo mineralization in the East Qinling Mo mineralization belt usually have Ce^{4+}/Ce^{3+} ratios varying from 53 to 278 with an average value of 120, indicating a less oxidized magma. This may account for the fact that Cu mineralization is generally absent in the East Qinling orogenic belt. It is reported so far that only the Jinduicheng Mo deposit in the belt contains 0.02 to 0.05% Cu in the ores (Liu and Yang, 2004).

Ore-bearing granite porphyries in the East Qinling Mo mineralization belt were considered to have inherited Mo from the source rocks (Lu et al., 2002). However, none of the crustal rock units in the East Qinling orogen contain significant Mo. The lower crusts in the southern margin of North China Craton, North Qinling, and Yangtze Block have 0.90, 2.04 and 0.52 ppm Mo, respectively (Gao et al., 1998); the lower crust in the southern margin of North China Craton and North Qinling units have Mo higher than the average continental lower crust (0.6 ppm) (Wedepohl, 1995). It is noteworthy that the bulk crusts in the southern margin of North China Craton, North Qinling, South Qinling and Yangtze Block have 0.79, 0.98, 0.54 and 0.68 ppm Mo, respectively (Gao et al., 1998), which are lower than the Mo concentration in continental crust of 1.1 ppm (Wedepohl, 1995). In addition, the Mo deposits in the East Qinling area mainly occur in the southern margin of North China Craton rather than the relatively Mo-enriched North Qinling units. Thus, the Mo mineralization in the East Qinling orogen is unlikely controlled by the basement. The enrichment of Mo in granitic melts is unlikely attributed to assimilation or remelting of the crustal material in the southern margin of North China Craton.

We consider that the Mo deposits may have sourced Mo from the mantle. The Mo-rich mantle may have formed beneath the southern margin of the North China Craton as a result of the Triassic continental crust subduction followed by dehydration of the crust and metasomatism of the mantle wedge. This is supported by the Cenozoic basaltic rocks in the southern margin of the North China Craton that are commonly enriched in Mo and have Mo contents ranging from 0.75 to

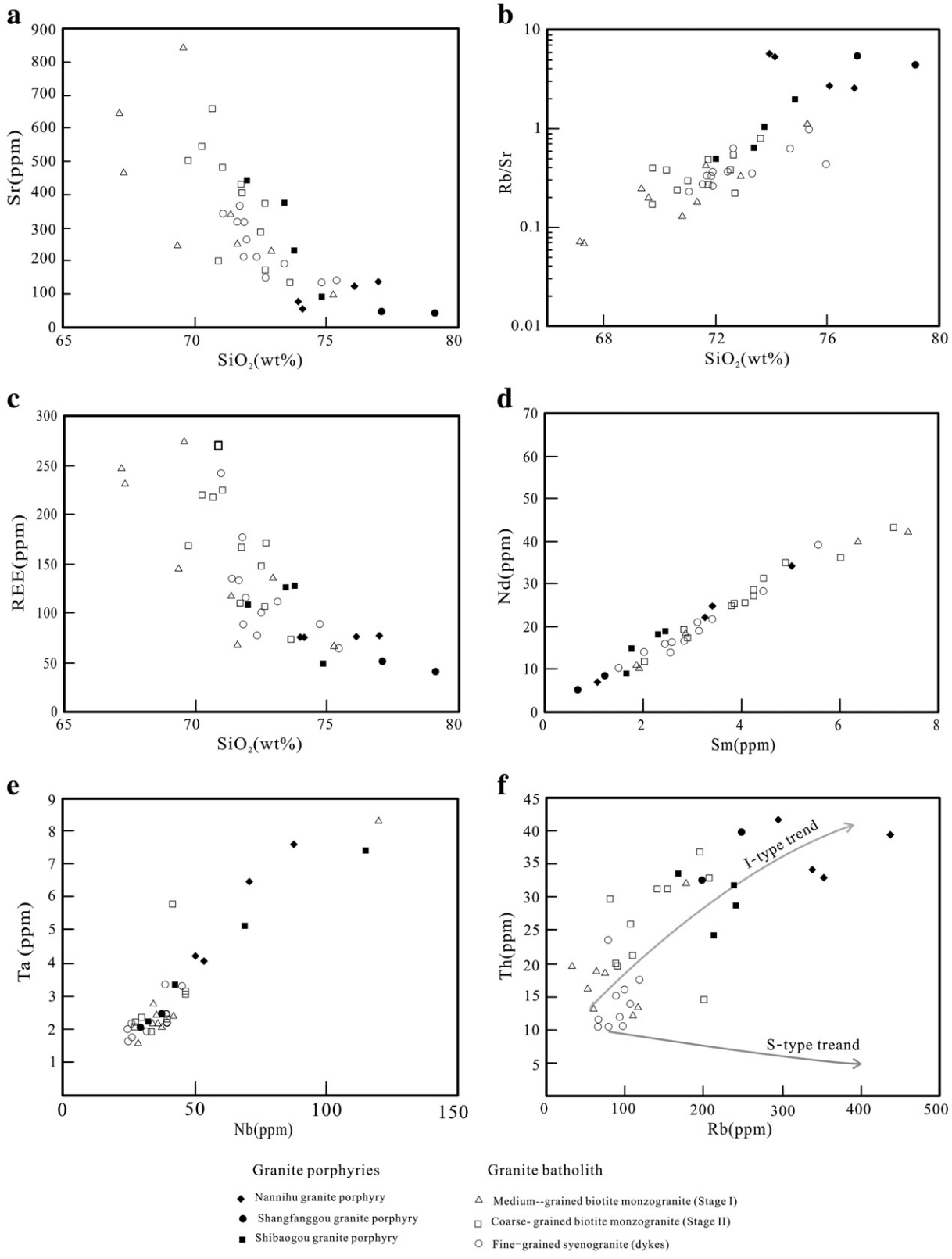

Fig. 8. Variations of trace elements for the granite porphyries in the Luanchuan ore field and the Heyu granite batholith.

7.21 ppm with an average value of 3.17 ppm (Yue et al., 2006). The existence of the enriched mantle source is also supported by the Late Triassic carbonatite associated with Mo deposit in East Qinling which is believed to be related to the underthrusting crustal material (Xu et al., 2010, 2011). The mantle wedge may also have been enriched in Mo by metasomatism during the subduction of the Yangtze Block (Xu

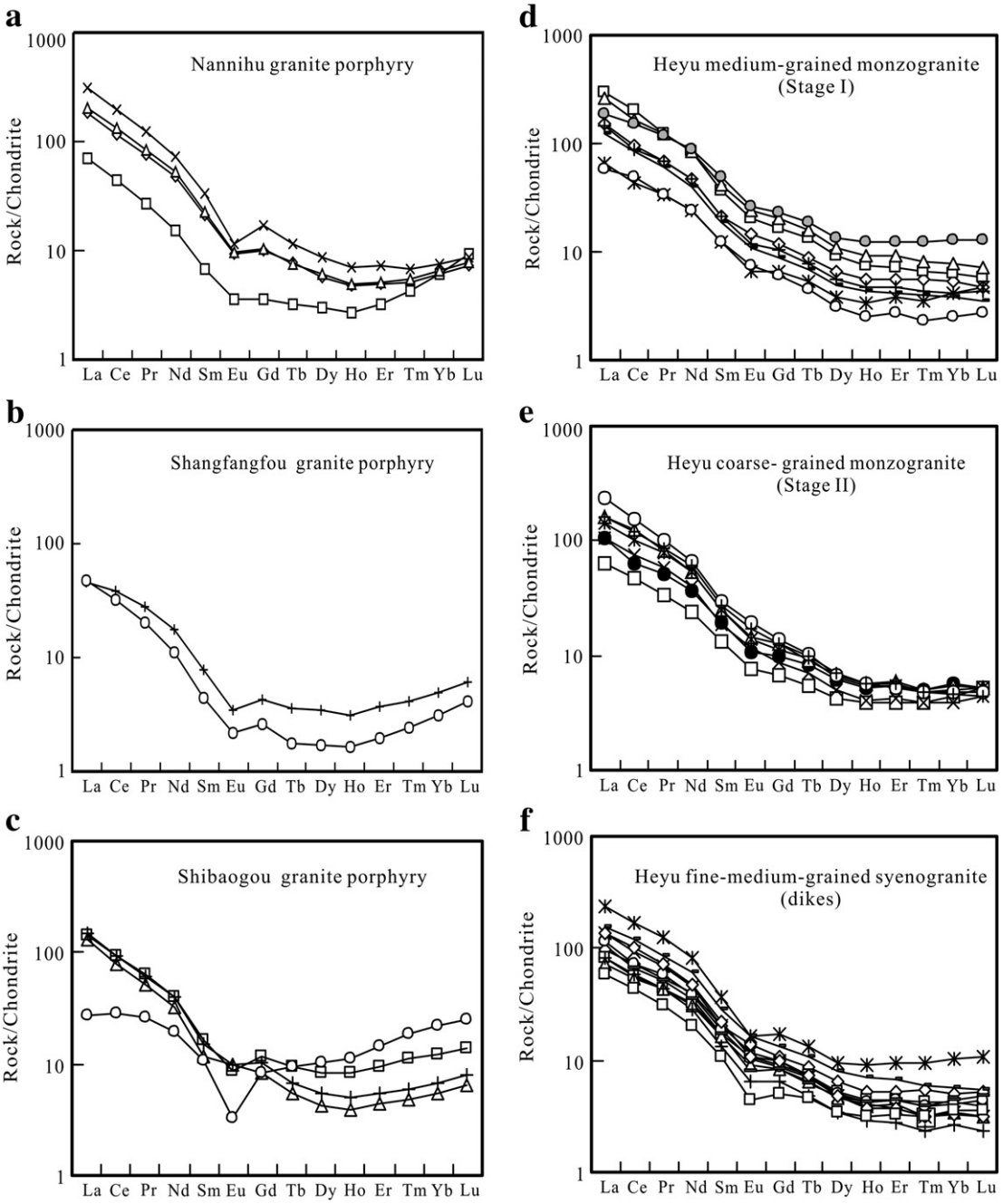

Fig. 9. Chondrite-normalized rare earth element patterns for the granite porphyries in the Luanchuan ore field and the Heyu granite batholith. Normalization values are from Sun and McDonough (1989).

et al., 2003b). Mesozoic mafic rocks, including the mafic dikes in the Luanchuan ore field and those in the southern and southeastern margins of the North China Craton have arc-like trace element signatures and high initial Sr isotopic ratios and negative $\varepsilon_{Nd}(t)$ values, indicating that they may have derived from enriched mantle sources (Yang et al., 2012b and references therein). The enriched mantle sources may have been generated by metasomatism of the overlying lithospheric mantle of the North China Craton by melts and/or fluids derived from the subducted Yangtze Block during the Triassic continental collision (e.g., Xu et al., 2004; Yang et al., 2012b, 2012c, 2013; Zhang et al., 2007; Zheng et al., 2012b). The delaminated lower continental crust of the North China Craton might also have contributed to the mantle enrichment (Gao et al., 2008; Yang et al., 2012c). Moreover, He–Ar isotopic composition of fluid inclusions in pyrites from the molybdenum deposits in the East Qinling Mo mineralization belt also support the involvement of the mantle component in the Mo mineralization (Zhu et al., 2009).

5. Conclusions

Mo-bearing granite porphyries in the Luanchuan ore field are formed in ~150 Ma and ~135 Ma, respectively, and are genetically linked to nearly coeval Heyu granite batholith. The Mo-bearing granite porphyries might represent the highly differentiated counterparts of

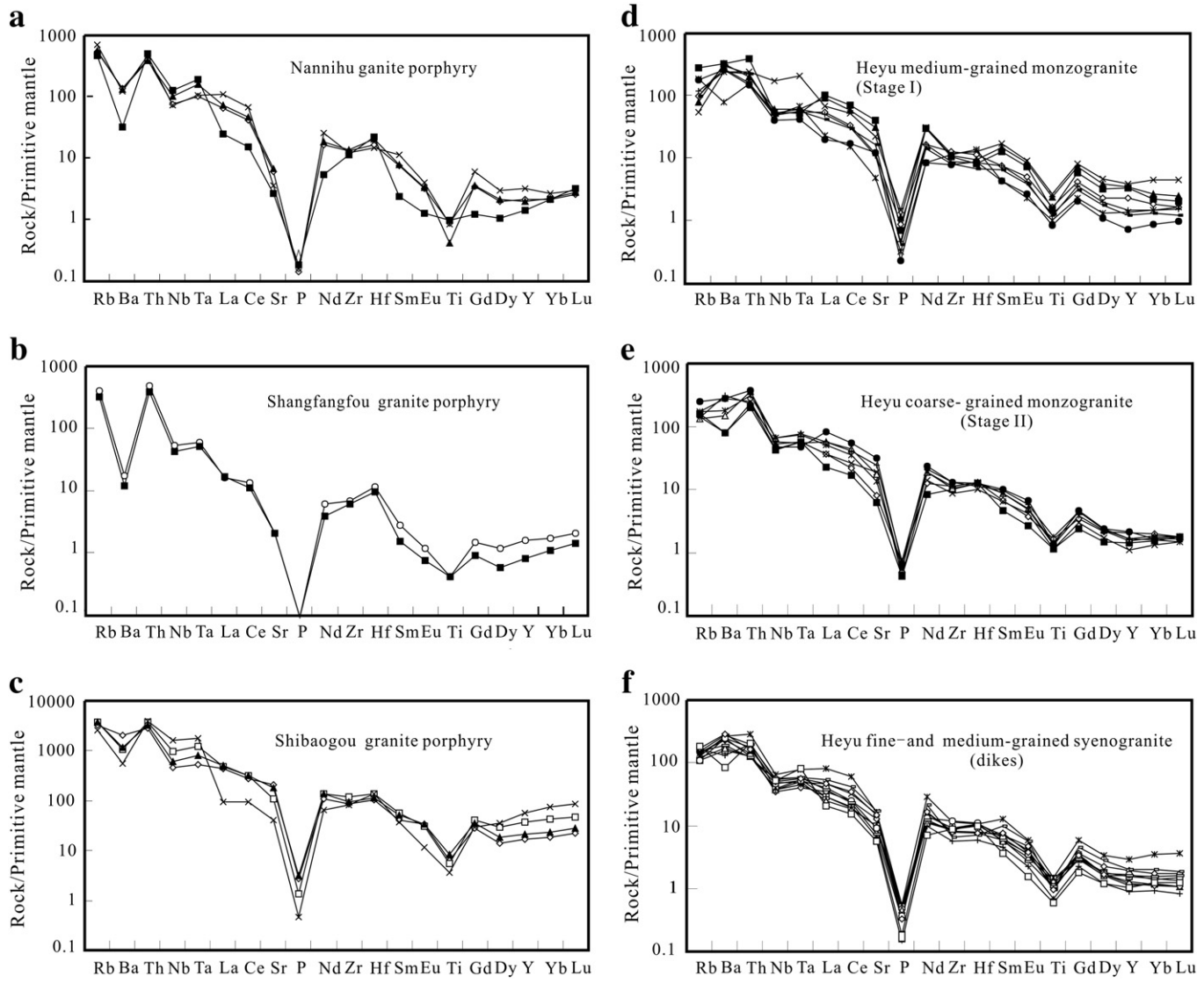

Fig. 10. Primitive mantle-normalized trace element patterns for the granite porphyries in the Luanchuan ore field and the Heyu granite batholith.
Normalization values are from Sun and McDonough (1989).

the Heyu batholith. The Mo-bearing granite porphyries and the Heyu granite batholith may have formed from remelting of the subducted crust of the Yangtze Block under a post-collisional tectonic setting. The interplay between the granitic melts and the melts and/or fluids from the enriched mantle wedge was probably responsible for the formation of the economic Mo deposits in the East Qinling Mo mineralization belt.

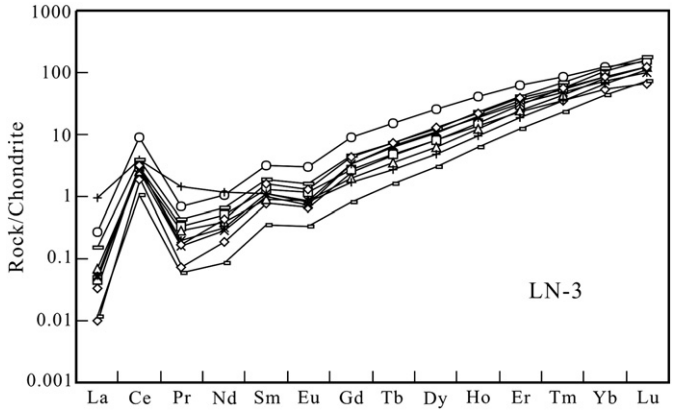

Fig. 11. Chondrite-normalized rare element element patterns of the zircons from the Nannihu granite porphyry.
Normalization values are from Sun and McDonough (1989).

Acknowledgment

This study was supported by NSFC grant (41372083) and the National Basic Research Program of China (973 Program No. 2012CB416602). We thank Prof. Xinxiang Lu and Dr. Zhenlei Yuan from the Henan Academy of Land and Resources, and Mr. Yaowu Song from the Henan Institute of Geological Survey for their assistance during field investigation. Many thanks go out to Dr. Gouchen Dong and two anonymous referees for their constructive comments that helped improve substantially the manuscript.

Appendix A. Analytical methods

A.1. Whole-rock major and trace elements

The Least altered samples from three granite porphyries in the Luanchuan orefield and the Heyu granite batholith were analyzed for major and trace elements. Major element contents of the granitic

Table 6
Trace element concentrations (ppm) of zircons from the Nannihu granite porphyry.

La	Ce	Pr	Nd	Sm	Eu	Gd	Tb	Dy	Ho	Er	Tm	Yb	Lu	Ce/Ce^*	Eu/Eu^*	Ce^{+4}/Ce^{+3}
0.01	1.16	0.01	0.09	0.12	0.04	0.51	0.17	2.07	0.79	3.83	0.90	9.23	1.71	28.4	0.49	79
0.05	1.83	0.03	0.24	0.20	0.07	0.55	0.18	2.05	0.87	4.99	1.43	17.7	4.08	11.6	0.65	120
0.07	1.59	0.027	0.18	0.14	0.05	0.40	0.13	1.60	0.70	4.02	1.12	13.6	3.17	9.0	0.65	164
0.05	1.53	0.02	0.13	0.15	0.04	0.67	0.23	2.72	1.12	5.73	1.39	14.7	3.06	11.9	0.39	122
0.05	1.84	0.02	0.15	0.17	0.05	0.7	0.24	2.81	1.08	5.31	1.22	12.4	2.52	14.3	0.44	93
0.27	5.51	0.07	0.48	0.48	0.17	1.85	0.58	6.43	2.31	10.4	2.22	20.9	3.87	9.8	0.55	53
0.93	2.33	0.14	0.54	0.17	0.05	0.34	0.10	1.19	0.53	3.11	0.88	11.0	2.85	1.6	0.64	155
0.01	0.66	0.01	0.04	0.05	0.02	0.17	0.06	0.77	0.36	2.09	0.60	7.43	1.87	16.2	0.64	278
0.15	2.37	0.04	0.31	0.28	0.09	0.93	0.28	3.21	1.31	6.91	1.74	19.95	4.41	7.50	0.54	82
0.03	1.98	0.02	0.20	0.25	0.07	0.89	0.28	3.24	1.27	6.32	1.43	14.5	3.14	19.8	0.45	59

Table 7
Sm–Nd isotopic compositions of the granite porphyries in the Luanchuan ore field and the Heyu granite batholith.

Sample no.	Nd (ppm)	Sm (ppm)	$^{147}Sm/^{144}Nd$	$^{143}Nd/^{144}Nd$	σ	t (Ma)	$\varepsilon_{Nd}(0)$	$\varepsilon_{Nd}(t)$	T_{DM} (Ma)	T_{DM2} (Ga)
Nannihu granite porphyry										
LN-1	22.120	3.251	0.08887	0.511775	11	150	−16.9	−14.8	1675	2.18
LN-2	7.200	1.031	0.08659	0.5118805	10	150	−14.8	−12.7	1520	2.00
LN-3	24.34	3.417	0.08489	0.511755	8	150	−17.3	−15.1	1647	2.21
LN-4	34.46	5.020	0.08809	0.5117385	8	150	−17.6	−15.5	1709	2.25
Shangfanggou granite porphyry										
LS-6	8.256	1.211	0.08870	0.5118055	10	135	−16.3	−14.4	1636	2.14
LS-9	5.189	0.686	0.07994	0.511852	10	135	−15.4	−13.4	1477	2.05
Shibaogou granite porphyry										
07-13	14.79	1.808	0.07392	0.511828	7	147.5	−15.8	−13.5	1439	2.07
07-15	18.37	2.337	0.07693	0.511844	7	147.5	−15.5	−13.3	1453	2.05
07-16	8.959	1.665	0.11238	0.511822	7	147.5	−16.0	−14.4	1991	2.15
Heyu medium-grained monzogranite (Stage I)										
HY10	3.300	22.10	0.09480	0.511781	7	148	−16.8	−14.8	1750	2.18
HY19	7.410	41.90	0.11220	0.511715	7	148	−18.0	−16.4	2147	2.32
HY41	1.860	11.40	0.10360	0.511719	7	148	−18.0	−16.2	1975	2.31
Heyu coarse-grained monzogranite (Stage II)										
HY38	3.840	25.60	0.09510	0.511745	7	135	−17.5	−15.7	1801	2.25
HY60	4.250	28.10	0.09590	0.511721	8	135	−17.9	−16.2	1844	2.30
Q9304-1[a]	7.734	55.95	0.08362	0.511707	6	135	−18.2	−16.3	1687	2.30
Q9304-2[a]	5.787	40.36	0.08674	0.511756	14	135	−17.2	−15.3	1670	2.22
Q9304-3[a]	5.194	37.26	0.08432	0.511646	8	135	−19.4	−17.5	1767	2.41
Q9304-4[a]	5.604	39.56	0.08568	0.511738	16	135	−17.6	−15.7	1677	2.25
Q9304-5[a]	4.898	32.97	0.08986	0.511803	15	135	−16.3	−14.5	1654	2.15
Heyu fine-grained monzogranite and syenogranite dikes										
HY28	2.620	15.20	0.10920	0.511982	9	135	−12.8	−11.3	1700	1.86
HY45	5.580	39.10	0.09070	0.511795	11	135	−16.5	−14.7	1675	2.16
HY53	1.630	9.530	0.10860	0.511835	8	135	−15.7	−14.2	1901	2.12

[a] Data from Zhang et al. (2006b).

rocks were determined by standard X-ray fluorescence (XRF) at the State Key Laboratory of Isotope Geochemistry, Guangzhou Institute of Geochemistry, Chinese Academy of Sciences (GIGCAS). Samples were prepared as glass discs using a Rigaku desktop fusion machine, formed by mixing 0.50 g of rock powder (dried at 110 C) with 4.0 g of lithium tetraborate for 15 min at 1100 °C in 95%Pt-5%Au crucibles. Analyses were performed on a Rigaku ZSX100e instrument. Calibration lines used in quantification were produced by bivariate regression of data from 36 reference materials encompassing a wide range of silicate compositions (Li et al., 2005b). Calibrations incorporated matrix corrections based on the empirical Traill-Lachance procedure, and analytical uncertainties are between 1% and 5%. A loss-on-ignition (LOI) measurement was undertaken on samples of dried rock powder by heating in a pre-ignition silica crucible to 1000 C for 1 h and recording the percentage weight loss.

Trace elements were analyzed using a Perkin-Elmer Sciex ELAN 6000 inductively coupled plasma mass spectrometer (ICP-MS) at the State Key Laboratory of Isotope Geochemistry, GIGCAS. The powdered samples (50 mg) were dissolved in _ ° screw-top Teflon beakers using an $HF+HNO_3$ mixture for 7 days at ~100 C. An internal standard solution containing the single element Rh was used to monitor drift in mass response during counting. USGS standard BCR-1 was used to calibrate the elemental concentrations of the measured samples. In-run analytical precision for most elements was better than 2%. The detailed procedures for trace element analysis by ICP-MS were described by Li (1997).

A.2. Whole-rock Nd isotope

Nd isotopic compositions were determined using a Micromass Isoprobe multi-collector ICP-MS at the State Key Laboratory of Isotope Geochemistry, GIGCAS, using analytical procedures described by Li et al. (2004). Nd fractions were separated by passing through cation columns followed by HDEHP columns, and the aqueous sample solution was taken up in 2% HNO3 and introduced into the MC-ICP-MS using a Meinhard glass nebuliser with an uptake rate of 0.1 ml/min. The inlet

Table 8
LA-MC-ICPMS zircon Hf isotopic compositions of the granite porphyries in the Lanchuan ore field and the Heyu granite batholith.

Spots	$^{176}Yb/^{177}Hf$	$^{176}Lu/^{177}Hf$	$^{176}Hf/^{177}Hf$	t (Ma)	$\varepsilon_{Hf}(t)$	$\varepsilon_{Hf}(0)$	T_{DM1} (Ga)	$f_{Lu/Hf}$	T_{DM2} (Ga)
Nannihu granite porphyry									
LN-3-1	0.022378	0.001007	0.281964	151	−25.4	−28.6	1.81	−0.97	2.80
LN-3-2	0.031203	0.001285	0.282081	148	−21.3	−24.4	1.66	−0.96	2.55
LN-3-3	0.031749	0.001387	0.281861	149	−29.1	−32.2	1.97	−0.96	3.03
LN-3-4	0.015746	0.000655	0.282209	150	−16.7	−19.9	1.46	−0.98	2.26
LN-3-5	0.031795	0.001650	0.282101	151	−20.6	−23.7	1.65	−0.95	2.50
LN-3-6	0.037763	0.001588	0.282133	149	−19.5	−22.6	1.60	−0.95	2.43
LN-3-7	0.023955	0.001104	0.282206	150	−16.9	−20.0	1.48	−0.97	2.27
LN-3-8	0.032958	0.001407	0.282100	150	−20.6	−23.8	1.64	−0.96	2.50
LN-3-9	0.023107	0.001167	0.281958	139	−25.9	−28.8	1.83	−0.96	2.83
LN-3-10	0.021701	0.001073	0.282327	150	−12.6	−15.7	1.31	−0.97	2.00
Shibaogou granite porphyry									
07-15-1	0.033113	0.001555	0.282130	144	−19.7	−22.7	1.60	−0.95	2.44
07-15-2	0.025541	0.001173	0.281968	147	−25.3	−28.4	1.81	−0.96	2.80
07-15-3	0.029486	0.001338	0.282162	137	−18.7	−21.6	1.55	−0.96	2.38
07-15-4	0.023110	0.001186	0.282240	147	−15.7	−18.8	1.43	−0.96	2.19
07-15-5	0.022713	0.001112	0.282152	147	−18.8	−21.9	1.55	−0.97	2.39
07-16-2	0.029780	0.001267	0.282298	150	−13.6	−16.8	1.36	−0.96	2.06
07-16-3	0.040693	0.001663	0.281985	142	−24.9	−27.8	1.81	−0.96	2.77
07-16-4	0.054203	0.002496	0.281698	145	−35.0	−38.0	2.27	−0.95	3.40
Heyu medium-grained monzogranite									
HY-14 01	0.013476	0.000515	0.281575	790	−25.2	−42.3	2.32	−0.98	3.26
HY-14 02	0.021425	0.000845	0.282120	145	−20.0	−23.1	1.59	−0.97	2.46
HY-14 03	0.022027	0.000882	0.282114	144	−20.2	−23.3	1.60	−0.97	2.47
HY-14 04	0.021103	0.000898	0.282110	158	−20.0	−23.4	1.60	−0.97	2.48
HY-14 05	0.014069	0.000607	0.282143	143	−19.2	−22.2	1.55	−0.98	2.41
HY-14 06	0.019433	0.000693	0.281435	136	−17.7	−47.3	2.52	−0.98	3.22
HY-14 07	0.024790	0.000927	0.282096	140	−20.9	−23.9	1.62	−0.97	2.52
HY-14 08	0.016979	0.000652	0.282101	151	−20.5	−23.7	1.61	−0.98	2.50
HY-14 09	0.020476	0.001037	0.282187	145	−17.6	−20.7	1.50	−0.97	2.31
HY-14 10	0.026096	0.001144	0.282172	146	−18.1	−21.2	1.53	−0.97	2.35
HY-14 11	0.024147	0.001095	0.282192	150	−17.3	−20.5	1.50	−0.97	2.30
HY-14 12	0.016617	0.000674	0.282152	145	−18.8	−21.9	1.54	−0.98	2.39
HY-14 13	0.018972	0.000805	0.282115	150	−20.0	−23.2	1.59	−0.98	2.47
HY-14 14	0.021934	0.001001	0.282169	149	−18.2	−21.3	1.53	−0.97	2.35
HY-14 15	0.023126	0.000902	0.281494	108	−22.1	−45.2	2.45	−0.97	3.28
HY-14 16	0.012523	0.000578	0.282139	148	−19.2	−22.4	1.55	−0.98	2.42
HY-14 17	0.017744	0.000721	0.282146	146	−19.0	−22.1	1.55	−0.98	2.40
HY-14 18	0.018279	0.000769	0.282156	150	−18.6	−21.8	1.53	−0.98	2.38
HY-14 19	0.032499	0.001134	0.282105	147	−20.5	−23.6	1.62	−0.97	2.49
HY-14 20	0.021701	0.000965	0.282148	147	−18.9	−22.1	1.55	−0.97	2.40
Heyu coarse-grained monzogranite									
HY-74 01	0.039532	0.001393	0.282125	140	−19.9	−22.9	1.60	−0.96	2.46
HY-74 02	0.072372	0.002622	0.282208	148	−17.0	−19.9	1.54	−0.92	2.27
HY-74 03	0.039778	0.001560	0.282168	143	−18.4	−21.4	1.55	−0.95	2.36
HY-74 04	0.048902	0.001786	0.282232	141	−16.2	−19.1	1.47	−0.95	2.22
HY-74 05	0.022681	0.000915	0.282347	135	−12.2	−15.0	1.27	−0.97	1.96
HY-74 06	0.073615	0.002621	0.282291	150	−14.0	−17.0	1.42	−0.92	2.09
HY-74 07	0.026239	0.001053	0.282203	128	−17.4	−20.1	1.48	−0.97	2.29
HY-74 08	0.030442	0.001255	0.281684	137	−35.6	−38.5	2.21	−0.96	3.43
HY-74 09	0.031102	0.001270	0.282241	140	−15.8	−18.8	1.44	−0.96	2.20
HY-74 10	0.029768	0.001182	0.282108	140	−20.5	−23.5	1.62	−0.96	2.49
HY-74 11	0.031171	0.001337	0.282115	134	−20.4	−23.2	1.62	−0.96	2.48
HY-74 12	0.015741	0.000743	0.282217	162	−16.2	−19.6	1.45	−0.98	2.23
HY-74 13	0.027993	0.001173	0.282198	160	−16.9	−20.3	1.49	−0.96	2.28
HY-74 14	0.021130	0.000840	0.282444	187	−7.6	−11.6	1.14	−0.97	1.71
HY-74 15	0.035713	0.001480	0.282177	155	−17.8	−21.0	1.53	−0.96	2.33
HY-74 16	0.014995	0.000551	0.282504	144	−6.4	−9.5	1.05	−0.98	1.60
HY-74 17	0.026085	0.001154	0.282241	140	−15.8	−18.8	1.43	−0.97	2.20
HY-74 18	0.047520	0.001921	0.282014	137	−24.0	−26.8	1.78	−0.94	2.71
HY-74 19	0.020365	0.000912	0.282186	146	−17.6	−20.7	1.50	−0.97	2.31
HY-74 20	0.029979	0.001163	0.281964	157	−25.3	−28.6	1.82	−0.96	2.80
Heyu fine-grained syenogranite dykes									
HY-73 01	0.034299	0.001356	0.282218	166	−16.1	−19.6	1.47	−0.96	2.23
HY-73 02	0.027186	0.001182	0.282203	168	−16.6	−20.1	1.49	−0.96	2.26
HY-73 03	0.033909	0.001360	0.282220	142	−16.5	−19.5	1.47	−0.96	2.24
HY-73 04	0.025342	0.001007	0.282185	137	−17.8	−20.8	1.50	−0.97	2.32
HY-73 05	0.045270	0.001808	0.282234	143	−16.1	−19.0	1.47	−0.95	2.21
HY-73 06	0.026943	0.001019	0.282214	130	−17.0	−19.7	1.46	−0.97	2.26
HY-73 07	0.045044	0.001785	0.282221	149	−16.4	−19.5	1.48	−0.95	2.24
HY-73 08	0.021302	0.000797	0.282174	668	−6.8	−21.1	1.51	−0.98	2.02
HY-73 09	0.018793	0.000723	0.282219	137	−16.6	−19.6	1.45	−0.98	2.24

(continued on next page)

Table 8 (*continued*)

Spots	$^{176}Yb/^{177}Hf$	$^{176}Lu/^{177}Hf$	$^{176}Hf/^{177}Hf$	t (Ma)	$\varepsilon_{Hf}(t)$	$\varepsilon_{Hf}(0)$	T_{DM1} (Ga)	$f_{Lu/Hf}$	T_{DM2} (Ga)
HY-73 10	0.024932	0.000961	0.282156	134	−18.9	−21.8	1.54	−0.97	2.39
Heyu fine-grained syenogranite dykes									
HY-73 11	0.017827	0.000762	0.282221	146	−16.4	−19.5	1.44	−0.98	2.23
HY-73 12	0.015188	0.000579	0.282160	138	−18.7	−21.6	1.52	−0.98	2.37
HY-73 13	0.044715	0.001605	0.282093	143	−21.0	−24.0	1.66	−0.95	2.53
HY-73 14	0.033878	0.001406	0.282288	148	−14.0	−17.1	1.38	−0.96	2.09
HY-73 15	0.030579	0.001186	0.282207	142	−17.0	−20.0	1.48	−0.96	2.27
HY-73 16	0.025299	0.001157	0.282172	196	−17.1	−21.2	1.53	−0.97	2.32
HY-73 17	0.029611	0.001136	0.282240	140	−15.9	−18.8	1.43	−0.97	2.20
HY-73 18	0.026027	0.001049	0.282266	569	−5.8	−17.9	1.39	−0.97	1.88
HY-73 19	0.051672	0.001852	0.282145	135	−19.4	−22.2	1.60	−0.94	2.42
HY-73 20	0.045553	0.001536	0.282181	150	−17.8	−20.9	1.53	−0.95	2.33

system was cleaned for 5 min between analyses using high purity 5% HNO_3 followed by a blank solution of 2% HNO_3. Measured $^{143}Nd/^{144}Nd$ ratios were normalized to $^{146}Nd/^{144}Nd = 0.7219$, and the reported $^{143}Nd/^{144}Nd$ ratios were further adjusted relative to the Shin Etsu JNdi-1 standard of 0.512115, corresponding to the La Jolla standard of 0.511860 (Tanaka et al., 2000).

A.3. Zircon U/Pb ages

Zircons were separated using conventional heavy liquid, magnetic separation techniques and then hand-picked. Cathodoluminescence (CL) images were obtained for zircons prior to analysis, using a JEOL JXA-8100 EPMA with Gatan Mono CL3 detector at State Key Laboratory

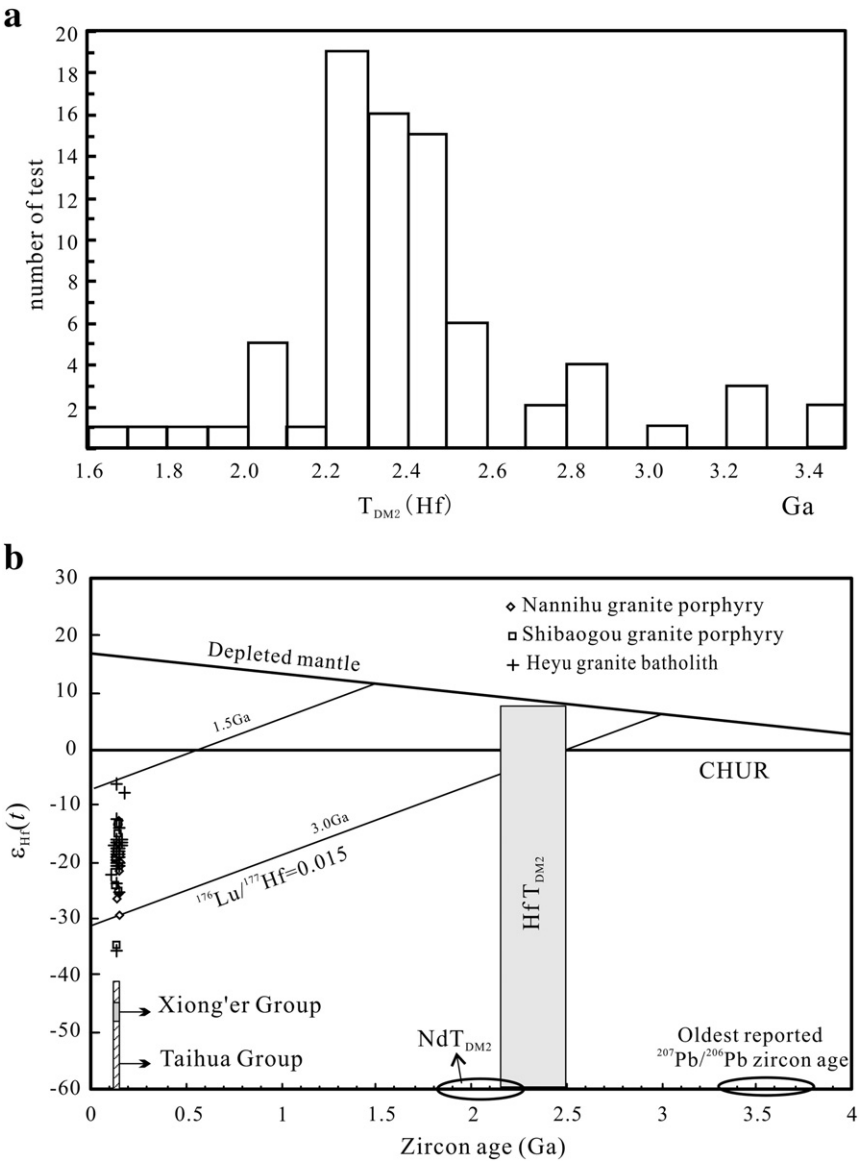

Fig. 12. A histogram of two-stage Hf model ages (a) and a plot of $\varepsilon_{Hf}(t)$ versus U/Pb ages (b) for the zircons from the Nannihu and Shibaogou granite porphyries and the Heyu granite batholith [ε_{Hf}(140 Ma) values of the Taihua and Xiong'er Groups are calculated based on the data of Diwu et al. (2010) and Wang et al. (2010), respectively.].

of Isotope Geochemistry, GIGCAS, in order to characterize internal structures and choose potential target sites for U-Pb dating.

Zircon U/Pb ages for the Nannihu and Shangfanggou granite porphyries were analyzed on an Agilent 7500a ICP-MS equipped with a 193 nm laser at the State Key Laboratory of Continental Dynamics, Northwest University, China. The ICP-MS used was an Elan 6100 DRC (Dynamic Reaction Cell) from Perkin Elmer/SCIX and the determinations were carried out in normal mode. During the analysis, the spot diameter was 30 pm. Raw count rates for ^{29}Si, ^{204}Pb, ^{206}Pb, ^{207}Pb, ^{208}Pb, ^{232}Th and 238 U were collected for age determination. U, Th and Pb concentrations were 29 calibrated by using Si as the internal calibrant and NIST SRM610 as the reference material. The ^{207}Pb/^{206}Pb and ^{206}Pb/^{238}U ratios were calculated using the GLITTER program, which then corrected using the Harvard zircon 91500 as external calibrant. Isotopic ratios and element concentrations are calculated using GLITTER program (version 4.0, Macquarie University); ages were calculated with Isoplot (version 2.49). The detailed analytical technique is described in Yuan et al.(2004). Zircons from the Heyu granites were analyzed for U-Pb dating and Hf isotopic composition at Institute of Geology and Geophysics, CAS, using Agilent 7500a ICPMS and Neptune MC-ICPMS equipped with Geolas 193nm excimer, following procedures described by Wu et al. (2006) and Xie et al. (2008).

Zircons from the Shibaogou granite porphyry were dated using a sensitive high-resolution ion microprobe (SHRIMP II) at the SHRIMP Center, Chinese Academy of Geological Sciences, Beijing. Instrumental conditions and data acquisition procedures are similar to those described by Williams and Claesson (1987), Compston et al. (1992), and Liu et al. (2003).

A.4. In situ zircon Lu-Hf isotope

In situ zircon Hf isotopic analysis was conducted using a Nu Plasma MC-ICP-MS, equipped with GeoLas 2005 excimer ArF laser ablation system, at State Key Laboratory of Continental Dynamics, Northwest University. Equipment parameters were set at: power=1300w, nebulizer gas=0.1 ml/min, auxiliary gas= 0.82 //min; plasma gas=13 L/min, He gas=1992sccm. During analysis, a laser repetition rate of 8 Hz was used and the spot size was 44 pm. Three standards, GJ-1, MON-1, and 91500, were exploited during the analysis using ^{176}Hf/^{177}Hf ratios of 0.282015, 282739, and 0.282307, respectively. Raw count rates for ^{172}Yb, ^{173}Yb, ^{175}Lu, ^{176}(Hf + Yb + Lu), ^{177}Hf, ^{178}Hf, ^{179}Hf, ^{180}Hf and ^{182}W were collected and isobaric 176 176 176 interference corrections for Lu and Yb on Hf were determined precisely. The ^{176}Lu/^{175}Lu=0.02655 and ^{176}Yb/^{172}Yb=0.58545 were used for the interference correction of ^{176}Hf and ^{176} Yb.

References

Ballard, J.R., Palin, J.M., Campbell, I.H., 2002. Relative oxidation states of magmas inferred from Ce(IV)/Ce(III) in zircon: application to porphyry copper deposits of northern Chile. Contrib. Mineral. Petrol. 144, 347–364.

Bao, Z.W., Zeng, Q.S., Zhao, T.P., Yuan, Z.L., 2009a. Geochemistry and petrogenesis of the ore-related Nannihu and Shangfanggou granite porphyries from east Qinling belt and their constraints on the molybdenum mineralization. Acta Petrol. Sin. 25, 2523–2536 (in Chinese with English abstract).

Bao, Z.W., Li, C.J., Qi, J.P., 2009b. SHRIMP zircon U–Pb age of the gabbro dyke in the Luanchuan Pb–Zn–Ag ore field, East Qinling orogen and its constraint on mineralization time. Acta Petrol. Sin. 25, 2951–2956 (in Chinese with English abstract).

Brueckner, H.K., 2009. Subduction of continental crust, the origin of post-orogenic granitoids (and anorthosites?) and the evolution of Fennoscandia. J. Geol. Soc. London 166, 753–762.

Candela, P.A., Bouton, S.L., 1990. The influence of oxygen fugacity on tungsten and molybdenum partitioning between silicate melts and ilmenite. Econ. Geol. 85, 633–640.

Carten, R.B., White, W.H., Stein, H.J., 1993. High-grade granite-related molybdenum systems: classification and origin. In: Kirkham, R.V., Sinclair, W.D., Thorpe, R.I., Duke, J.M. (Eds.), Mineral Deposit Modeling. Geological Association of Canada, Special Paper, 40, pp. 521–554.

Chen, J.F., Guo, X.S., Tang, J.F., Zhou, T.X., 1999. Nd isotopic model ages: implications of the growth of the continental crust of southeastern China. J. Nanjing Univ. (Nat. Sci.) 35, 649–658 (in Chinese with English abstract).

Chen, Y.J., Li, C., Zhang, J., Wang, H.H., 2000. Sr and O isotopic characteristics of porphyries in the Qinling molybdenum deposit belt and their implication to genetic mechanism and type. Sci. China D 43 (SI), 82–94.

Collins, W.J., 1998. Evaluation of petrogenetic models for Lachlan fold belt granitoids: implications for crustal architecture and tectonic models. Aust. J. Earth Sci. 45, 483–500.

Compston, W., Williams, I.S., Kirschvink, J.L., Zhang, Z., Ma, G., 1992. Zircon U–Pb ages for the Early Cambrian time-scale. J. Geol. Soc. London 149, 171–184.

Corfu, F., Hanchar, J.M., Hoskin, P.W.O., Kinny, P., 2003. Atlas of zircon textures. Rev. Mineral. Geochem. 53, 469–500.

Diwu, C.R., Sun, Y., Lin, C.L., Wang, H.L., 2010. LA-(MC)-ICPMS U–Pb zircon geochronology and Lu–Hf isotope compositions of the Taihua complex on the southern margin of the North China Craton. Chin. Sci. Bull. 55, 2557–2571.

Dong, Y.P., Zhang, G.W., Neubauer, F., Liu, X.M., Genser, J., Hauzenberger, C., 2011. Tectonic evolution of the Qinling orogen. China: review and synthesis. J. Asian Earth Sci. 41, 213–237.

Frost, B.R., Barnes, C.G., Collins, W.J., Arculus, R.J., Ellis, D.J., Frost, C.D., 2001. A geochemical classification for granitic rocks. J. Petrol. 42, 2033–2048.

Gao, S., Luo, T.C., Zhang, B.R., Zhang, H.F., Han, Y.W., Zhao, Z.D., Hu, Y.K., 1998. Chemical composition of the continental crust as revealed by studies in East China. Geochim. Cosmochim. Acta 62, 1959–1975.

Gao, S., Rudnick, R.L., Xu, W.L., Yuan, H.L., Liu, Y.S., Puchtel, I., Liu, X., Huang, H., Wang, X.R., 2008. Recycling deep cratonic lithosphere and generation of intraplate magmatism. Earth Planet. Sci. Lett. 270, 41–53.

Gao, X.Y., Zhao, T.P., Yuan, Z.L., Zhou, Y.Y., Gao, J.F., 2010. Geochemistry and petrogenesis of the Heyu batholith in the southern margin of the North China block. Acta Petrol. Sin. 26, 3485–3506 (in Chinese with English abstract).

Gray, C.M., 1984. An isotopic mixing model for the origin of granitic rocks in southeastern Australia. Earth Planet. Sci. Lett. 70, 47–60.

Guo, B., Zhu, L.M., Li, B., Gong, J.H., Wang, J.Q., 2009. Zircon U–Pb age and Hf isotope composition of the Huashan and Heyu granite plutons at the southern margin of North China Craton: implications for geodynamic setting. Acta Petrol. Sin. 25, 265–281 (in Chinese with English abstract).

Guo, P., Santosh, M., Li, S.R., 2013. Geodynamics of gold metallogeny in the Shandong Province, NE China: an integrated geological, geophysical and geochemical perspective. Gondwana Res. 24, 1172–1202.

Hoskin, P.W.O., Schaltegger, U., 2003. The composition of zircon and igneous and metamorphic petrogenesis. Rev. Mineral. Geochem. 53, 27–62.

Hou, G.T., Wang, Y.X., Hari, K.R., 2010. The Late Triassic and Late Jurassic stress fields and tectonic transmission of North China Craton. J. Geodyn. 50, 318–324.

Hu, S.X., Lin, Q.L., Chen, Z.M., 1988. Geology and metallogeny of the collision belt between the South China and North China plates. Nanjing University Press, Nanjing (1–558 pp., in Chinese).

Huang, J., Zheng, Y.F., Zhao, Z.F., Wu, Y.B., Zhou, J.B., Liu, X.M., 2006. Melting of subducted continent: element and isotopic evidence for a genetic relationship between Neoproterozoic and Mesozoic granitoids in the Sulu orogen. Chem. Geol. 229, 227–256.

Huang, X.L., Niu, Y.L., Xu, Y.G., Yang, Q.J., Zhong, J.W., 2010. Geochemistry of TTG and TTG-like gneisses from Lushan–Taihua complex in the southern North China Craton: implications for Late Archaean crustal accretion. Precambrian Res. 182, 43–56.

Jiang, N., Guo, J.H., Chang, G.H., 2013. Nature and evolution of the lower crust in the eastern North China Craton: a review. Earth Sci. Rev. 122, 1–9.

Li, S.G., Liu, D.L., Chen, Y.Z., 1994. Neodymium isotopic compositions of continental crust in the northern margin of Yangtze Block and its tectonic implications. Geochimica 23, 10–17 ((suppl.)(in Chinese with English abstract)).

Li, X.H., 1997. Geochemistry of the Longsheng ophiolite from the southern margin of Yangtze Craton, SE China. Geochem. J. 31, 323–337.

Li, X.H., Liu, D.Y., Sun, M., Li, W.X., Liang, X.R., Liu, Y., 2004. Precise Sm–Nd and U–Pb isotopic dating of the super-giant Shizhuyuan polymetallic deposit and its host granite, Southeast China. Geol. Mag. 141, 225–231.

Li, Y.F., Mao, J.W., Hu, H.B., Guo, B.J., Bai, F.J., 2005a. Geology, distribution, types and tectonic settings of Mesozoic molybdenum deposits in East Qinling area. Miner. Deposita 24, 292–304 (in Chinese with English abstract).

Li, X.H., Qi, C.S., Liu, Y., Liang, X.R., Tu, X.L., Xie, L.W., Yang, Y.H., 2005b. Petrogenesis of the Neoproterozoic bimodal volcanic rocks along the western margin of the Yangtze Block: new constraints from Hf isotopes and Fe/Mn ratios. Chin. Sci. Bull. 50, 2481–2486.

Li, Y.F., Mao, J.W., Bai, F.J., Li, J.P., He, Z.J., 2006. Re–Os isotopic dating of molybdenites in the Nannihu molybdenum (tungsten) ore field in the eastern Qinling and its geological significance. Geol. Rev. 49, 652–659 (in Chinese with English abstract).

Li, N., Chen, Y.J., Zhang, H., Zhao, T.P., Deng, X.H., Wang, Y., Ni, Z.Y., 2007. Molybdenum deposits in East Qinling. Earth Sci. Front. 14, 186–198 (in Chinese with English abstract).

Li, N., Chen, Y.J., Ni, Z.Y., Hu, H.Z., 2009a. Characteristics of ore-forming fluids of the Yuchiling porphyry Mo deposit, Songxian county, Henan Province, and its geological significance. Acta Petrol. Sin. 25, 2509–2522 (in Chinese with English abstract).

Li, N., Chen, Y.J., Sun, Y.L., Hu, H.Z., Li, J., Zhang, H., Ni, Z.Y., 2009b. Molybdenite Re–Os isochron age of the Yuchiling porphyry Mo deposit, Henan Province and its geological implications. Acta Petrol. Sin. 25, 413–421 (in Chinese with English abstract).

Li, H.Y., Mao, J.W., Wang, X.X., Ye, H.S., Yang, L., 2011. Sr, Nd, Pb isotopic characteristics of granite in Jinduicheng area and their geological significance. Geol. China 38, 1536–1550 (in Chinese with English abstract).

Li, D., Zhang, S.T., Yan, C.H., Wang, G.W., Song, Y.W., Ma, Z.B., Han, J.W., 2012a. Late Mesozoic time constraints on tectonic changes of the Luanchuan Mo belt, East Qinling orogen, Central China. J. Geodyn. 61, 94–104.
Li, C.Y., Wang, F.Y., Hao, X.L., Ding, X., Zhang, H., Ling, M.X., Zhou, J.B., Li, Y.L., Fan, W.M., Sun, W.D., 2012b. Formation of the world's largest molybdenum metallogenic belt: a plate-tectonic perspective on the Qinling molybdenum deposits. Int. Geol. Rev. 54, 1093–1112.
Li, N., Chen, Y.J., Pirajno, F., Gong, H.J., Mao, S.D., Ni, Z.Y., 2012c. LA-ICP-MS zircon U–Pb dating, trace element and Hf isotope geochemistry of the Heyu granite batholith, eastern Qinling, Central China: implications for Mesozoic tectono-magmatic evolution. Lithos 142–143, 34–47.
Li, N., Chen, Y.J., Pirajno, F., Ni, Z.Y., 2013a. Timing of the Yuchiling giant porphyry Mo system, and implications for ore genesis. Miner. Deposita 48, 505–524.
Li, S.R., Santosh, M., Zhang, H.F., Shen, J.F., Dong, G.C., Wang, J.H., Zhang, J.Q., 2013b. Inhomogeneous lithospheric thinning in the central North China Craton: zircon U–Pb and Se–He–Ar isotopic record from magmatism and metallogeny in the Taihang Mountains. Gondwana Res. 23, 141–160.
Liang, H.Y., Campbell, I.H., Allen, C., Sun, W.D., Liu, C.Q., Yu, H.X., Xie, Y.W., Zhang, Y.Q., 2006. Zircon Ce^{4+}/Ce^{3+} ratios and ages for Yulong ore-bearing porphyries in eastern Tibet. Miner. Deposita 41, 152–159.
Ling, W.L., Ren, B.F., Duan, R.C., Lin, X.M., Ma, X.W., Peng, L.H., Liu, Z.X., Cheng, J.P., Yang, H.M., 2008. Timing of the Wudangshan, Yaolinghe volcanic sequences and mafic sills in South Qinling: U–Pb zircon geochronology and tectonic implication. Chin. Sci. Bull. 53, 2192–2199.
Liu, Y.Y., Yang, Q.L., 2004. Comprehensive recovery of Cu, Fe, S from tailings of the Jinduicheng Mo deposit. China Mine Eng. 33 (3), 15–17 (in Chinese with English abstract).
Liu, D., Jian, P., Zhang, Q., Zhang, F.Q., Shi, Y.R., Zhang, L.Q., Tao, H., 2003. SHRIMP dating of adakites in the Tulingkai ophiolite, Inner Mongonia: evidence for the Early Paleozoic subduction. Acta Geol. Sin. 77, 317–327.
Liu, Y.C., Fu, G.Z., Gao, F., Jin, Y.H., Zhao, Y.L., 2006. Geological character research of ore-forming mother rock of Nannihu oversize molybdenum ore deposit of Luanchuan in Henan. China Molybd. Ind. 30 (3), 13–17 (in Chinese with English abstract).
Liu, Y.C., Jin, Y.H., Ban, Y.H., Wu, F., Fu, Z.G., Zhang, P., 2007. The distribution law of bearing ore stratum in East Qinling–Dabie mountain mineralization belt. China Molybd. Ind. 31 (1), 12–17 (in Chinese with English abstract).
Lu, X.X., Yu, Z.P., Feng, Y.L., Wang, Y.T., Ma, W.F., Cui, H.F., 2002. Mineralization and tectonic setting of deep-hypabyssal granites in east Qinling mountains. Miner. Deposita 21, 168–178 (in Chinese with English abstract).
Lu, F.X., Wang, C.Y., Hu, B.Q., Wu, Q.F., Zheng, J.P., 2003. Structure of the lower crust and detachment and subduction of the lithosphere of the South Qinling. Geol. China 30, 113–119 (in Chinese with English abstract).
Lu, X.X., Wang, C.Y., Zheng, Y.F., 2004. Lithospheric composition and structure beneath the northern margin of the Qinling orogenic belt — on deep-seated xenoliths in Minggang region of Henan Province. Sci. China D 47, 13–22.
Luo, M.J., Zhang, F.M., Dong, Q.Y., 1991. Molybdenum Deposits in China. Hennan Science and Technology Press, Zhengzhou (118–128 pp., in Chinese).
Luo, M.J., Lin, Q.L., Lu, X.X., Chen, T.H., 1993. Geological characteristics of the molybdenum mineralized granites in east Qinling. Henan Geol. 11 (1), 2–8 (in Chinese with English abstract).
Mao, J.W., Goldfarb, R.J., Zhang, Z.W., Xu, W.Y., Qiu, Y.M., Deng, J., 2002. Gold deposits in the Xiaoqinling–Xiong'ershan region, Qinling mountains, Central China. Miner. Deposita 37, 306–325.
Mao, J.W., Xie, G.Q., Zhang, Z.H., Li, X.F., Wang, Y.T., Zhang, C.Q., Li, Y.F., 2005. Mesozoic large-scale metallogenic pulses in North China and corresponding geodynamic setting. Acta Petrol. Sin. 21, 169–188 (in Chinese with English abstract).
Mao, J.W., Xie, G.Q., Bierlein, F., Qu, W.J., Du, A.D., Ye, H.S., Pirajno, F., Li, H.M., Guo, B.J., Li, Y.F., Yang, Z.Q., 2008. Tectonic implications from Re–Os dating of Mesozoic molybdenum deposits in the East Qinling–Dabie orogenic belt. Geochim. Cosmochim. Acta 72, 4607–4626.
Mao, J.W., Ye, H.S., Wang, R.T., Dai, J.Z., Jian, W., Xiang, J.F., Zhou, K., Meng, F., 2009. Mineral deposit model of Mesozoic porphyry Mo and Vein-type Pb–Zn–Ag ore deposits in the eastern Qinling, Central China and its implication for prospecting. Geol. Bull. China 28, 72–79 (in Chinese with English abstract).
Mao, J.W., Xie, G.Q., Pirajno, F., Ye, H.S., Wang, Y.B., Li, Y.F., Xiang, J.F., Zhao, H.J., 2010. Late Jurassic–Early Cretaceous granitoid magmatism in Eastern Qinling, central-eastern China: SHRIMP zircon U–Pb ages and tectonic implications. Aust. J. Earth Sci. 57, 51–78.
Meng, Q.R., Zhang, G.W., 1999. Timing of collision of the North and South China blocks: controversy and reconciliation. Geology 27, 123–126.
Meng, Q.R., Zhang, G.W., 2000. Geologic framework and tectonic evolution of the Qinling orogen, Central China. Tectonophysics 323, 193–196.
Ouyang, J.P., Zhang, B.R., 1996. Geochemical evidence for the formation and evolution of North Qinling microcontinent. Sci. China D 39, 43–49.
Oyarzun, R., Marquez, A., Lillo, J., Lopez, I., Rivera, S., 2002. Reply to Discussion on "Giant versus small porphyry copper deposits of Cenozoic age in northern Chile: adakitic versus normal calc-alkaline magmatism" by Oyarzun, R., Marquez, A., Lillo, J., Lopez, I., Rivera, S. (Mineralium Deposita 36, 794–798, 2001). Miner. Deposita 37, 795–799.
Ratschbacher, L., Hacker, B.R., Calvert, A., Webb, L.E., Grimmer, J.C., McWilliams, M.O., Ireland, T., Dong, S.W., Hu, J.M., 2003. Tectonics of the Qinling (Central China): tectonostratigraphy, geochronology, and deformation history. Tectonophysics 366, 1–53.
Shi, Y.X., Li, N., Yang, Y., 2009. Ore geology and fluid inclusion geochemistry of the Sandaozhuang Mo–W deposit in Luanchuan County, Henan Province. Acta Petrol. Sin. 25, 2575–2587 (in Chinese with English abstract).
Sillitoe, R.H., 1980. Types of porphyry molybdenum deposits. Min. Mag. 142 (550–551), 553.
Sun, X.M., Liu, X.S., 1987. Study on the relationship between two different types of granites and their genesis in Jinduicheng molybdenum mining area, Shaanxi Province. Contrib. Geol. Miner. Resour. Res. 2 (2), 34–45 (in Chinese with English abstract).
Sun, S.-s., McDonough, W.F., 1989. Chemical and isotopic systematics of oceanic basalts: implications for mantle compositions and processes. In: Saunders, A.D., Norry, M.J. (Eds.), Magmatism in the Ocean Basins. Geological Society, London, pp. 313–345.
Sun, W.D., Ding, X., Hu, Y.H., Li, Z.H., 2007. The golden transformation of the Cretaceous plate subduction of the in the west Pacific. Earth Planet. Sci. Lett. 262, 533–542.
Tanaka, T., Togashi, S., Kamioka, H., Amakawa, H., Kagami, H., Hamamoto, T., Yuhara, M., Orihashi, Y., Yoneda, S., Shimizu, H., Kunimaru, T., Takahashi, K., Yanagi, T., Nakano, T., Fujimaki, H., Shinjo, R., Asahara, Y., Tanimizu, M., Dragusanu, C., 2000. JNdi-1: a neodymium isotopic reference in consistency with La Jolla neodymium. Chem. Geol. 168, 279–281.
Vigneresse, J.L., 2007. The role of discontinuous magma inputs in felsic magma and ore generation. Ore Geol. Rev. 30, 181–216.
Walsh, E.O., Hacker, B.R., 2004. The fate of subducted continental margins: two-stage exhumation of the high-pressure to ultrahigh-pressure Western Gneiss Region, Norway. J. Metamorph. Geol. 22, 671–687.
Wang, X.X., Jiang, C.Y., An, S.Y., 1986. The characteristics of two-pyroxene granulite enclaves in the mid-acid porphyry bodies and their geological significance. J. Chang'an Univ. (Earth Sci. Ed.) 8 (2), 16–21 (in Chinese with English abstract).
Wang, C.M., Deng, J., Zhang, S.T., Ye, H.S., 2006. Endogentic metallogenic system of Nannihu Mo–W–Cu–Pb–Zn–Ag–Au ore-forming area. Geol. Sci. Technol. Inf. 25 (6), 47–52 (in Chinese with English abstract).
Wang, X.L., Jiang, S.Y., Dai, B.Z., 2010. Melting of enriched Archean subcontinental lithospheric mantle: evidence from the ca. 1760 Ma volcanic rocks of the Xiong'er Group, southern margin of the North China Craton. Precambrian Res. 182, 204–216.
Wang, L.J., Griffin, W.L., Yu, J.H., O'Reilly, S.Y., 2013. U–Pb and Lu–Hf isotopes in detrital zircon from Neoproterozoic sedimentary rocks in the northern Yangtze Block: implications for Precambrian crustal evolution. Gondwana Res. 23, 1261–1272.
Watson, E.B., Harrison, T.M., 1983. Zircon saturation revisited: temperature and composition effects in a variety of crustal magma types. Earth Planet. Sci. Lett. 64, 295–304.
Wedepohl, K.H., 1995. The composition of the continental crust. Geochim. Cosmochim. Acta 59, 1217–1232.
Wei, Q.G., Gao, X.Y., Zhao, T.P., Chen, W., Yang, Y.H., 2010. Petrogenesis of Tangjiaping granite porphyry in northern Dabie: evidence from zircon LA-ICPMS U–Pb dating and geochemical characteristics. Acta Petrol. Sin. 26, 1550–1562 (in Chinese with English abstract).
Williams, I.S., Claesson, S., 1987. Isotopic evidence for the Precambrian provenance and Caledonian metamorphism of high grade paragneisses from the Seve Nappes, Scandinavian Caledonides: II. Ion microprobe zircon U–Th–Pb, Contrib. Mineral. Petrol. 97, 205–217.
Wu, Y.B., Zheng, Y.F., 2013. Tectonic evolution of a composite collision orogen: an overview on the Qinling Tongbai–Hong'an–Dabie–Sulu orogenic belt in Central China. Gondwana Res. 23, 1402–1428.
Wu, F.Y., Yang, Y.H., Xie, L.W., Yang, J.H., Xu, P., 2006. Hf isotopic compositions of the standard zircons and baddeleyites used in U–Pb geochronology. Chem. Geol. 234, 105–126.
Wu, F.Y., Xu, Y.G., Gao, S., Zheng, J.P., 2008. Lithospheric thinning and destruction of the North China Craton. Acta Petrol. Sin. 24, 1145–1174 (in Chinese with English abstract).
Xie, L.W., Zhang, Y.B., Zhang, H.H., Sun, J.F., Wu, F.Y., 2008. In situ simultaneous determination of trace elements, U–Pb and Lu–Hf isotopes in zircon and baddeleyite. Chin. Sci. Bull. 53, 1565–1573.
Xu, W.C., Pang, Z.S., Zhou, Q.M., Wang, X.H., Yang, G.Q., 2003a. Metallogeny of silver–lead–zinc polymetallic ores outside Nannihu molybdenum (tungsten) ore field, Luanchuan County, Henan Province and its prospective. Miner. Resour. Geol. 17, 198–202 (in Chinese with English abstract).
Xu, J.H., Yang, Y.L., Wang, L.J., Zhu, H.P., Wang, L.Q., 2003b. Trace element in CO_2 fluid inclusions in mantle lherzolite. Acta Petrol. Sin. 19, 307–313 (in Chinese with English abstract).
Xu, Y.G., Ma, J.L., Huang, X.L., Iizuka, Y., Chung, S.L., Wang, Y.B., Wu, X.Y., 2004. Early Cretaceous gabbrioc complex from Yinan, Shandong province: petrogenesis and mantle domains beneath the North China Craton. Int. J. Earth Sci. 93, 1025–1041.
Xu, W.L., Gao, S., Yang, D.B., Pei, F.P., Wang, Q.H., 2009. Geochemistry of eclogite xenoliths in Mesozoic adakitic rocks from Xuzhou–Suzhou area in Central China and their tectonic implications. Lithos 107, 269–280.
Xu, C., Kynicky, J., Chakhmouradian, A.R., Qi, L., Song, W.L., 2010. A unique Mo deposit associated with carbonatites in the Qinling orogenic belt, Central China. Lithos 118, 50–60.
Xu, C., Taylor, R.N., Kynicky, J., Chakhmouradian, A.R., Song, W.L., Wang, L.J., 2011. The origin of enriched mantle beneath North China block: evidence from young carbonatites. Lithos 127, 1–9.
Xue, F., Lerch, M.F., Kroner, A., Reischmann, T., 1996. Tectonic evolution of the east Qinling Mountains, China, in the Palaeozoic: a review and new tectonic model. Tectonophysics 253, 271–284.
Yan, C.H., 2004. Study on Inner Structure of Lead–Zinc–Silver Mineralization System in Eastern Qinling. Geological Publishing House, Beijing (1–96 pp., in Chinese with English abstract).
Yang, R.Y., Xu, Z.W., Ren, Q.J., 1997. Ages and magma sources of Shibaogou and Huoshenmiao complexes in East Qinling. Bull. Miner. Petrol. Geochem. 16 (1), 15–18 (in Chinese with English abstract).

Yang, J.S., Xu, Z.Q., Pei, X.Z., Shi, R.D., Wu, C.L., Zhang, J.X., Li, H.B., Meng, F.C., Rong, H., 2002. Discovery of diamond in North Qinling: evidence for a giant UHPM belt across Central China and recognition of Paleozoic and Mesozoic dual deep subduction between North China and Yangtze Plates. Acta Geol. Sin. 76, 484–495 (in Chinese with English abstract).

Yang, Y., Zhang, J., Yang, Y.F., Shi, Y.X., 2009a. Characteristics of fluid inclusions and its geological implication of the Shangfanggou Mo deposit in Luanchuan county, Henan province. Acta Petrol. Sin. 25, 2563–2574 (in Chinese with English abstract).

Yang, Y.F., Li, N., Yang, Y., 2009b. Fluid inclusion study of the Nannihu porphyry Mo–W deposit, Luanchuan County, Henan Province. Acta Petrol. Sin. 25, 2550–2562 (in Chinese with English abstract).

Yang, X.Y., Lu, X.X., Du, X.W., Li, W.M., Zhang, Z.W., Qu, W.J., 2010. Ore geochemistry, petrogenesis and metallogenic dynamic of the Nangou molybdenum district in the east Qinling orogenic belt. Acta Geol. Sin. 84, 1049–1079 (in Chinese with English abstract).

Yang, Y., Wang, X.X., Ke, C.H., Li, J.B., 2012a. Zircon U–Pb age, geochemistry and Hf isotopic compositions of Shibaogou granitoid pluton in the Nannihu ore district, western Henan Province. Geol. China 39, 1525–1542 (in Chinese with English abstract).

Yang, Q.L., Zhao, Z.F., Zheng, Y.F., 2012b. Modification of subcontinental lithospheric mantle above continental subduction zone: constraints from geochemistry of Mesozoic gabbroic rocks in southeastern North China. Lithos 146–147, 164–182.

Yang, D.B., Xu, W.L., Pei, F.P., Yang, C.H., Wang, Q.H., 2012c. Spatial extent of the influence of the deeply subducted South China Block on the southeastern North China Block: constraints from Sr–Nd–Pb isotopes in Mesozoic mafic igneous rocks. Lithos 136–139, 246–260.

Yang, Q.Y., Santosh, M., Shen, J.F., Li, S.R., 2013. Juvenile vs. recycled crust in NE China: zircon U–Pb geochronology, Hf isotope and an integrated model for Mesozoic gold mineralization in the Jiaodong Peninsula. Gondwana Res. http://dx.doi.org/10.1016/j.gr.2013.06.003.

Yao, J.M., Zhao, T.P., Li, J., Sun, Y.L., Yuan, Z.L., Chen, W., Han, J., 2009. Molybdenite Re–Os age and zircon U–Pb age and Hf isotope geochemistry of the Qiyugou gold system, Henan Province. Acta Petrol. Sin. 25, 374–384 (in Chinese with English abstract).

Yue, K.F., He, Y., Dong, Z.X., Zhang, W.P., 2006. Molybdenum content of mantle-derived rocks from South China block and southern margin of North China Craton in eastern China and its implications. Geochimica 35, 388–394 (in Chinese with English abstract).

Zhang, L.G., 1988. Lead isotopic compositions of feldspar and ore and their geologic significance. Miner. Deposita 7 (2), 55–64 (in Chinese with English abstract).

Zhang, L.G., Wang, K.F., 1991. Studies of Mesozoic–Cenozoic tectonic isotopic geology in eastern China. J. Guilin Coll. Geol. 11 (1), 35–48 (in Chinese with English abstract).

Zhang, S.B., Zheng, Y.F., 2007. Growth and reworking of the Yangtze continental nucleus: evidence from zircon U–Pb ages and Hf isotopes. Acta Petrol. Sin. 23, 393–402 (in Chinese with English abstract).

Zhang, B.R., Li, Z.J., Luo, T.C., Gu, X.M., 1987. Regional Geochemistry of Lushi–Lingbao District, West Henan. Geological Publishing House, Beijing (1–285 pp., in Chinese with English abstract).

Zhang, H.F., Zao, Z.D., Luo, T.C., Zhang, B.R., 1995. Crustal growth and lower crust nature of North Qinling: study of Sm–Nd isotopic model ages. Acta Petol. Sin. 11, 160–170 (in Chinese with English abstract).

Zhang, G.W., Meng, Q.G., Yu, Z.P., Sun, Y., Zhou, D.W., Guo, A.L., 1996. Orogenesis and dynamics of the Qinling orogen. Sci. China D 39, 225–234.

Zhang, H.F., Zhang, B.R., Ling, W.L., Gao, S., Ouyang, J.P., 1997. Late Proterozoic crustal accretion of south Qinling: Nd isotopic study from granitic rock. Geochimica 26, 16–23 (in Chinese with English abstract).

Zhang, S.B., Zheng, Y.F., Wu, Y.B., Zhao, Z.F., Gao, S., Wu, F.Y., 2006a. Zircon U–Pb age and Hf isotope evidence for 3.8 Ga crustal remnant and episodic reworking of Archean crust in South China. Earth Planet. Sci. Lett. 252, 56–71.

Zhang, Z.Q., Zhang, G.W., Liu, D.Y., Wang, Z.Q., Tang, S.H., Wang, J.H., 2006b. Geochronology and Geochemistry of Ophiolites, Granitoids and Clastic Rocks in Qinling Orogen. Geological Publishing House, Beijing 178–180 (in Chinese).

Zhang, H.F., Ying, J.F., Shimoda, G., Kita, N.T., Morishita, Y., Shao, J.A., Tang, Y.J., 2007. Importance of melt circulation and crust–mantle interaction in the lithospheric evolution beneath the North China Craton: evidence from Mesozoic basalt-borne clinopyroxene xenocrysts and pyroxenite xenoliths. Lithos 96, 67–89.

Zhang, R.Y., Liou, J.G., Ernst, W.G., 2009. The Dabie–Sulu continental collision zone: a comprehensive review. Gondwana Res. 16, 1–26.

Zhang, Y.H., Mao, J.W., Jian, W., Li, Z.Y., 2010. Present status of research on molybdenum deposit in eastern Qinling and the problems remained. Global Geol. 29, 188–202 (in Chinese with English abstract).

Zhao, Z.F., Zheng, Y.F., 2009. Remelting of subducted continental lithosphere: petrogenesis of Mesozoic magmatic rocks in the Dabie–Sulu orogenic belt. Sci. China D 52, 1295–1318.

Zheng, J.P., Griffin, W.L., O'Reilly, S.Y., Hu, B.Q., Zhang, M., Tang, H.Y., Su, Y.P., Zhang, Z.H., Pearson, N., Wang, F.Z., Lu, F.X., 2008. Continental collision and accretion recorded in the deep lithosphere of Central China. Earth Planet. Sci. Lett. 269, 496–506.

Zheng, Y.F., Yu, C.M., Su, Y.P., Tang, H.Y., Wei, Q.R., Zhang, Z.H., Lu, F.X., 2009. Mesozic zonal lithosphere beneath the southern margin of the North China: significance for continental formation and evolution. Earth Sci. J. China Univ. Geosci. 34, 28–34 (in Chinese with English abstract).

Zheng, T.Y., Zhu, R.X., Zhao, L., Ai, Y.S., 2012a. Intralithospheric mantle structures recorded continental subduction. J. Geophys. Res. 117, B03308.

Zheng, J.P., Griffin, W.L., Ma, Q., O'Reilly, S.Y., Xiong, Q., Tang, H.Y., Zhao, J.H., Yu, C.M., Su, Y.P., 2012b. Accretion and reworking beneath the North China Craton. Lithos 149, 61–78.

Zhou, K., Ye, H.S., Mao, J.W., Qu, W.J., Zhou, S.F., Meng, F., Gao, Y.L., 2009. Geological characteristics and molybdenite Re–Os isotopic dating of Yuchiling porphyry Mo deposit in western Henan Province. Miner. Deposita 28 (2), 170–184 (in Chinese with English abstract).

Zhu, L.M., Zhang, G.W., Guo, B., Lee, B., 2009. He–Ar isotopic system of fluid inclusions in pyrite from the molybdenum deposits in south margin of North China Block and its trace to metallogenetic and geodynamic background. Chin. Sci. Bull. 54 (14), 2479–2492.

Zhu, L.M., Zhang, G.W., Guo, B., Lee, B., Gong, H.J., Wang, F., 2010a. Geochemistry of the Jinduicheng Mo-bearing porphyry and deposit, and its implications for the geodynamic setting in East Qinling, P.R. China. Chem. Erde 70, 159–174.

Zhu, G., Niu, M.L., Xie, C.L., Wang, Y.S., 2010b. Sinistral to normal faulting along the Tan–Lu Fault Zone: evidence for geodynamic switching of the East China continental margin. J. Geol. 118, 277–293.